Theoretical and Applied Climatology
https://doi.org/10.1007/s00704-021-03752-4

ORIGINAL PAPER

Surface-based nocturnal air temperature inversions in southern Poland and their influence on PM_{10} and $PM_{2.5}$ concentrations in Upper Silesia

Tadeusz Niedźwiedź[1] · Ewa Bożena Łupikasza[1] · Łukasz Małarzewski[1] · Tomasz Budzik[1]

Received: 2 February 2021 / Accepted: 5 August 2021

Abstract

The frequency, strength and seasonal variations of surface-based temperature inversions (SBTIs) in Upper Silesia (Southern Poland) were examined using data from January 2001 to September 2020. Based on the air temperatures recorded at the meteorological station of the Institute of Earth Sciences in Sosnowiec (263 m a.s.l.) at heights of 2 m and 88 m above the ground, the vertical temperature gradient of the 100-m layer ($\gamma_{\mathrm{Sos}}100$ m) was determined. A lapse rate of $\gamma_{\mathrm{Sos}}100\ \mathrm{m} > 0.5$ K was defined as a temperature inversion. The measurements for 00 UTC (midnight) and 12 UTC (midday) were compared with data from the upper air station in Wrocław (116 m a.s.l.) located in the Lower Silesia Lowland, approximately 170 km NW of Sosnowiec. Based on soundings from Wrocław, in addition to the temperature gradient in the lower 100-m layer of air ($\gamma_{\mathrm{Wrc}}100$), three other characteristics of SBTIs were calculated: inversion depth (ID) or thickness in metres, inversion strength (ΔT_{i}) in K and vertical temperature gradients across the whole SBTI layer γ_{i} in K 100 m^{-1}. On an annual basis, the frequency of nighttime SBTIs ($\gamma > 0.5$ K 100 m^{-1}) ranged from 47% in Sosnowiec to almost 59% in Wrocław. At both stations, the fewest SBTIs occurred in winter (23–38%) and the most in summer (64–75%). Moreover, they were more frequent in spring (52–61%) than in autumn (49–59%). The SBTI frequency was very low during the midday hours, amounting to 0.6–0.7% days a year, and it increased to 1–2% only in winter. Annually, the depth of 81% of inversions ranged between 50 and 300 m, varying seasonally from almost 67% in winter to 87% in summer. The presented research shows that SBTIs in winter were among the main factors contributing to a high concentration of particulate matter pollutants in the ground-level atmosphere. During nights with temperature inversions, the annual mean PM_{10} concentration reached 125% of the mean value, ranging from 114% in summer to 189% in winter.

1 Introduction

Air pollution is one of the critical problems in urban areas. Oppressive and health-endangering conditions are associated with episodes of high air pollution concentrations enhanced by air temperature inversions (ATIs). An ATI occurs when the air temperature increases with altitude (Glickman 2000). Surface-based temperature inversions (SBTIs) are typical features of the atmospheric boundary layer and occur mostly at night (Zhang et al. 2011; Wang and Wang 2014; Fochesatto 2015). An SBTI usually forms because the lowest layer of the troposphere cools due to the strong irradiance of heat from the ground surface, and as a result, air temperature increases with height. Sometimes, inversions have an advection-radiative character, if warmer airflow is observed mostly from the S-SW sector, above the cooled ground layer. The rate of this increase sometimes reaches 5–10 K per 100 m. Under such conditions, there is a strong descent of air leading to the extreme concentration of particulate matter in the near-ground layer. Thus, SBTIs prevent dispersion and lead to an increase in air pollutant concentrations, particularly in winter (Janhäll et al. 2006; Milionis and Davies 2008; Olofson et al. 2009; Bokwa 2011; Zhang et al. 2011; Gramsch et al. 2014; Malingowski et al. 2014; Wang and Wang 2014; Li et al. 2015; Largeron and Staquet 2016; Czarnecka and Nidzgorska-Lencewicz 2017; Czarnecka et al. 2019).

The vertical structure of air temperature in the lowest part of the atmospheric boundary layer in urban conditions

✉ Tadeusz Niedźwiedź
tadeusz.niedzwiedz@us.edu.pl

[1] Faculty of Natural Sciences, Institute of Earth Sciences, University of Silesia in Katowice, Będzińska street 60, 41-200, Sosnowiec, Poland

Published online: 09 September 2021

has infrequently been discussed in the literature (Wolf et al. 2014) due to the specific information (vertical measurements) it requires, but the problem is of high importance. The lapse rate can be used to determine the mixing layer height and atmospheric stability, both of which help to understand the distribution of air pollution at the surface-based layer of the atmosphere (Wang and Wang 2014).

The existing studies usually use data from short-lasting experiments (Janhäll et al. 2006) or weather stations located at various altitudes (e.g. Largeron and Staquet 2016). Vertical temperature profiles were also obtained by installing temperature sensors on masts, e.g. in Moscow (Lokoshchenko 2002), in Kraków (Bokwa 2011) and in Hamburg up to a height of 280 m (Brümmer et al. 2012; Brümmer and Schultze 2015). The vertical temperature structure in the lowest 1000 m of the atmosphere in the Bergen valley, Norway (Wolf et al. 2014), over 2 years was obtained by a microwave temperature profiler. The boundary layer structure was also researched based on radiosonde observations (Seidel et al. 2010; Wang and Wang 2014). Based on data from radiosondes, detailed studies on inversion climatology were carried out for Łeba (northern Poland) on the Baltic coast (Czarnecka et al. 2019), Germany (Gutsche 1983), Prague in the Czech Republic (Stryhal et al. 2017), Athens in Greece (Katsoulis 1988; Prezerakos 1998; Kassomenos and Koletsis 2005), Oman (Abdul-Wahab et al. 2004), Teheran in Iran (Tavousi and Abadi 2016), China (Li et al. 2019) and the Arctic (Kahl 1990; Bradley et al. 1992; Serreze et al. 1992; Bourne et al. 2010; Malingowski et al. 2014). Palarz et al. (2018) investigated the climatology of SBTIs in Europe based on reanalysis.

There are a few studies that link air pollution concentrations to air temperature inversions and circulation types (Sheridan et al. 2008; Caputa et al. 2009; Leśniok and Caputa 2009; Leśniok et al. 2010; Kassomenos et al. 2014a, b; Grundström et al. 2015a, b; Li et al. 2015; Largeron and Staquet 2016; Pleijel et al. 2016; Liu et al. 2017). According to these studies, the PM_{10} concentration depends on the persistence and strength of the air temperature inversions that systematically occur during a high-pressure regime (Largeron and Staquet 2016). The near-ground accumulation of aerosols particles is more strongly affected by anticyclonic patterns than by cyclonic patterns. Moreover, Grundström et al. (2015a, b) found a strong association between low wind speeds, positive vertical temperature gradients and air pollution concentrations in Sweden. These authors also investigated the relationship between particle number concentration and other air pollutants (NO_x, NO_2 and PM_{10}) using Lamb (1972) weather types. In the USA, there is also a significant linkage between tropical and polar weather types and air pollutant concentrations (Liu et al. 2017). The high air pollution episode that occurred on 4 to 11 February 2005, in Sosnowiec (southern Poland) was related to southeastern and southern air advection under the influence of a high-pressure system and an accompanying air temperature inversion (Widawski 2015).

The Upper Silesia Region is one of the most polluted regions in Poland. Exceptionally high concentrations of air pollutants commonly occur in winter during air temperature inversions. For example, the strongest SBTI (11.8 K) was recorded on 23 December 2010, at 5:40 UTC. According to the Inspectorate of Environmental Protection in Katowice on that night, the PM_{10} concentration reached 219 $\mu g \cdot m^{-3}$ in Dąbrowa Górnicza and 377 $\mu g\ m^{-3}$ in Katowice and exceeded 700 $\mu g \cdot m^{-3}$ in Rybnik. Another episode of high air pollution concentrations occurred in Sosnowiec on 8 February 2015, during an air temperature inversion. That time, the SBTI strength reached more than 8 K 100 m^{-1}, and the maximum hourly concentrations of PM_{10} and SO_2 equalled 414 $\mu g\ m^{-3}$ and 189 $\mu g\ m^{-3}$, respectively. An even more extreme case occurred on 9 January 2017, in association with a high-pressure wedge and polar air masses over the region. That day was frosty with an average air temperature of − 19.2 °C. At night, the SBTI was as strong as 8.1 K 100 m^{-1}. This situation led to an extremely high concentration of air pollution. According to the Voivodship Inspectorate of Environmental Protection, the concentration of PM_{10} amounted to 985 $\mu g\ m^{-3}$ in Dąbrowa Górnicza (11 p.m.) and 667 $\mu g\ m^{-3}$ in Katowice (4 a.m.).

The study aims to determine the climatology of SBTIs in the lowest (approximately 100 m) ground layer of the atmosphere in the centre of one of the most urbanized areas in Poland (Śląsko-Zagłębiowska Metropolis) and to recognize their strength, spatial extent and impact on particulate matter concentrations. The representativeness of the measurements in Sosnowiec for southern Poland was assessed using data from radiosonde measurements from Wrocław representing Low Silesia Lowland in SW Poland. The study is based on unique, long-term data, thus delivering results that are also significant from a statistical point of view. The results of this study can be used for modelling and predicting air quality (Janhäll et al. 2006; Li et al. 2015; Liu et al. 2017).

2 Data and methods

The research area covers the large Górnośląsko-Zagłębiowska Metropolis (GZM) in Poland and is considered to be the most polluted region in Central Europe. The GZM is located in southern Poland in the Silesian Upland. Approximately, a dozen cities are concentrated in the centre of this district. Urban and industrial complexes are interconnected via an extensive network of roads and railway lines with dense public transport. In winter, the area is frequently affected by episodes of high air pollutant concentrations. Radiosounding data come from Wrocław that represents

Lower Silesian Lowland in SW Poland. It is one of the warmest regions of Poland (Woś 2010) with mean annual temperature (1951–2000) exceeding 8.3 °C and monthly temperatures between − 1.5 °C in January to 18.1 °C in July. Upper Silesian climatic region is a little cooler than Lower Silesia with the annual temperature reaching 8.1 °C (− 2.4 °C in January and 17.8 °C in July). The upland location of Upper Silesia is also manifested by much higher annual rainfall in this region (675 mm) compared to the eastern climatic region of Lower Silesia (570 mm), as well as a number of days with precipitation (respectively from 175 to 159 days) and snow cover (64 to 49 days).

2.1 Meteorological and air pollution data

The meteorological data were taken from the station located in Sosnowiec (50°17.49′N, 19°08.02′E) at an altitude of 263 m above sea level. This station has been operating since 1993 at ground level. The vertical measurements of air temperature (every 10 min) started in 1996 after installing the second station located approximately 5 m above the roof of the building at a height of 88 m above the ground (Fig. 1). The building hardly impacts the measurements since the temperature and humidity sensors are placed on the platform mounted approximately 5 m above the roof surface. Thus, the database used in this study contains meteorological data from two levels (2 m and 88 m above ground). We used the almost 20-year long time series covering the period from January 2001 to September 2020. Measurement data is stored with a time resolution of 10 min. However, in this study, we included hourly data to compare them with air pollution data. For comparison with radiosounding air temperature from Wrocław, we used data from 00 and 12 UTC.

The sensors type HMP45D of Vaisala (Finland) sheltered with a radiation protection shelters RPD14 were used to measure the air temperature and relative humidity. Temperature measurements resistive platine sensors PT100. Their accuracy is ± 0.2 K. Before the installation of sensors on the 2 m and 88 m levels above the ground, they were calibrated to each other. Temperature sensors were re-calibrated every time they were replaced approximately every 3-5 years and after any station failures. The quality check of the data set was performed after each month on the basis of comparative graphs of the temperature course with resolution of 10 minutes. There was no significant influence of the building heating on the air temperature values at the upper station, as the sensors were located about 5 m above the roof of the building at its western end. Stronger winds at the 88-m level than at the lower station also counteracted the heating influence of the building on the sensor readings. This is

Fig. 1 Location of the research area and measuring points. The photograph shows the building of the Institute of Earth Sciences and meteorological stations located in Sosnowiec at near the ground level (2 m) and 5 m above the roof of the building, DG, Dąbrowa Górnicza; Sos, Sosnowiec; Kce, Katowice; Zbrz, Zabrze; Gce, Gliwice

evidenced by the course of air temperature at both stations in periods without temperature inversion. In these situations, the temperature at 88 m was always about 0.5–1.5 K lower than at the bottom station. The dataset on the vertical profile of air temperature and humidity in Sosnowiec is unique in Poland. Photographs of the meteorological station and graphics showing the real-time measurements are available on the following websites: https://www.us.edu.pl/instytut/inoz/ogrodek-meteorologiczny-us/ and https://www.meteo.us.edu.pl/start/inwersj.

We also used hourly and daily meteorological data from a synoptic station in the Katowice-Muchowiec local airport (WMO no 12560; 50°14′N, 19°02′E, $Hs = 284$ m above sea level (a.s.l.)) included in the measurement network of the Institute of Meteorology and Water Management-National Research Institute (IMWM-NRI). The station is located approximately 9 km to SW from Sosnowiec (Fig. 1).

The data from Sosnowiec did not allow the SBTI height to be assessed. To do so and to assess the spatial extent of the SBTI, the data from Sosnowiec were compared with the upper air soundings from the Wrocław IMWM-NRI station (WMO number 12 425 Wrocław-I 51.13°N, 16.98°E, $Hs = 116$ m above sea level) located in the Lower Silesia Lowland, approximately 170 km NW of Sosnowiec (Fig. 1). The SBTIs simultaneously occurring at both stations were recognized as regional-scale inversions, while the SBTIs occurring at one of these stations were assumed to be local in character. The soundings only exist two times per day (00 UTC and 12 UTC) and cover the period between January 2001 and September 2020. But for 12 UTC, there is no data for the years 2001 and 2002. The sounding data were downloaded from the database of upper air soundings provided by the University of Wyoming, Department of Atmospheric Sciences (http://weather.uwyo.edu/upperair/soundings.html). In the case of gaps, Wrocław's series was completed with data from the Prostejov station (WMO number 11 747, 49.15°N, 17.13°E, $Hs = 216$ m above sea level) in the Czech Republic, located approximately 165 km SW of Sosnowiec. The accuracy of air temperature measured by radiosondes is currently about ± 0.1 K (Stryhal et al. 2017).

The hourly data on air pollution come from the archives of the Central Inspectorate of Environmental Protection (http://www.powietrze.gios.gov.pl/pjp/archives) measured by a net of professional monitoring stations belonging to the Voivodship Inspectorate of Environmental Protection in Katowice (www.katowice.wios.gov.pl). We studied the data on the concentration of coarse particulate matter PM_{10} (diameter of particles < 10 μm) from 5 monitoring stations (Table 1, Fig. 1) covering the period from January 2001 to September 2020. Data concerning fine particulate matter $PM_{2.5}$ (diameter of particles < 2.5 μm) have only been available for Katowice only since June 2009. The accuracy of measurements is about ± 1 $\mu g \cdot m^{-3}$. All these monitoring stations are typical urban (75%) and industrial (25%), evenly distributed throughout the Górnośląsko-Zagłębiowska Metropolis (Leśniok et al. 2010) over an area of approximately 50 × 30 km. The sources of pollution are both industrial works, road transport and domestic in winter.

2.2 Classification of circulation types and air masses

Circulation types and air masses also influence the inversion depth and intensity (Prezerakos 1998; Caputa et al. 2009; Kassomenos et al.2014a) as well as air pollution concentration (Sheridan et al. 2008; Leśniok and Caputa 2009; Leśniok et al. 2010; Widawski 2015; Pleijel et al. 2016; Liu et al. 2017). For Southern Poland, we have in the Institute of Earth Science (University of Silesia) archive calendar of circulation types since September 1876 and air masses since December 2000, prepared and updated by T. Niedźwiedź (available on request by e-mail: tadeusz.niedzwiedz@us.edu.pl). The classification of circulation types was partly based on the typology of atmospheric circulation developed by Lamb (1972) for the British Isles, with some modifications for non-advective situations in particular. Synoptic maps of Europe were used to determine the direction of air mass advection (N, NE, E, SE, S, SW, W, NW) and baric system type (a, anticyclonic situation; c, cyclonic situation). In addition to the sixteen advective situations, two non-advective anticyclonic types were distinguished: Ca, central anticyclonic situation and Ka, high wedge or anticyclonic ridge, and two cyclonic types with differentiated

Table 1 Location of the air pollution monitoring stations of the Voivodship Inspectorate of Environmental Protection in Katowice included in the paper

Station name	Address	International code	Latitude °N	Longitude °E	Altitude m a.s.l
Dąbrowa Górnicza	Tysiąclecia str. 25a	PL0237A	50.320	19.231	293
Sosnowiec	Lubelska str. 51	PL0529A	50.286	19.184	250
Katowice	Kossutha str. 6	PL0008A	50.265	18.975	273
Zabrze	M. Skłodowskiej-Curie str. 34	PL0242A	50.316	18.772	255
Gliwice	Mewy str. 34	PL0238A	50.279	18.656	236

advection: Cc, central cyclonic situation and Bc, cyclonic trough. Baric cols and low-gradient situations are marked with an "*x*" (Twardosz and Niedźwiedź 2001). Thus, the entire classification includes twenty-one types (ten anticyclonic types, ten cyclonic types and one indefinite type). Model synoptic maps for individual types of circulation can be found in the publication by Twardosz et. al. (2011) in Fig. 2 on pages 235–236.

We also used geographical classification of air masses (Glickman 2000) that indicates the source area of air masses inflowing to southern Poland and their thermal and moisture properties marked with c, continental; m, maritime and w, warm (Niedźwiedź and Łupikasza 2019). The weather in southern Poland during the period 1951–2020 is conditioned on about 58% of days by humid polar-sea air masses off the Atlantic. They are distinct for containing fresh polar maritime air (Pm 18%), old transformed polar maritime air (Pmo 32%) and warm polar maritime air (Pmw 8%) flowing in from areas of the Atlantic between Madeira and the British Isles or from the Mediterranean basin. Dry polar continental air (Pc) from over Russia flows in for about 21% of the days. Cold Arctic air (A) flows in 8% days a year. Warm tropical air (T) appears most rarely (3%). Days with mixed air masses were recorded for approximately 10% of days a year.

2.3 Surface-based air temperature inversion characteristics and methods of their determination

To select days with SBTIs, the differences between air temperatures registered at heights of 88 m above the ground (T_{88m}) and 2 m (T_{2m}) were calculated ($\Delta T_{86m} = T_{88m} - T_{2m}$). These differences describing the thermal structure of the atmosphere were extrapolated by multiplying ΔT_{86m} by 1.16 (100/86 = 1.16) to obtain a lapse rate (γ_{Sos}100 m) defined as a change in air temperature expressed in K per 100 m. The analogous lapse rate was also calculated for Wrocław (γ_{Wrc}100 m) based on temperature soundings.

A positive lapse rate ($\gamma > 0$) indicates an inversion, while a negative lapse rate stands for normal conditions—a decrease in air temperature in line with an increase in altitude. Compensating possible measurement errors, we adopted the thresholds of ± 0.5 K for isothermal conditions (see below). The lapse rates (γ) were classified into the following six classes of air stability:

1. Strong instability	$\gamma < -1.0$ K 100 m^{-1}
2. Conditioned instability	-1.0 K 100 m$^{-1} \leq \gamma < -0.5$ K 100 m^{-1}
3. Isothermal conditions	-0.5 K 100 m$^{-1} \leq \gamma \leq 0.5$ K 100 m^{-1}
4. Weak inversion	1.0 K 100 m$^{-1} > \gamma > 0.5$ K 100 m^{-1}
5. Moderate inversion	5.0 K 100 m$^{-1} > \gamma \geq 1.0$ K 100 m^{-1}
6. Strong inversion (strong stability)	$\gamma \geq 5.0$ K 100 m^{-1}

Based on soundings, two main characteristics of SBTIs were calculated for Wrocław: inversion depth ($ID = h_i - h_0$) in metres (from the surface h_0 to the inversion top h_i—the level with the highest temperature in the vertical profile) and inversion strength or intensity ($\Delta T_i = T_{hi} - T_{h0}$) in K. Vertical temperature gradients across the whole SBTI layer γ_i in K 100 m^{-1} were also calculated after formula: $\gamma_i = \Delta T_i / ID * 100$. The SBTI with a temperature gradient of $\gamma_i > 0.5$ K 100 m^{-1} were selected for further analysis. Figure 2 presents a vertical profile of air temperature in Wrocław with typical nocturnal inversions. The basic characteristics of the SBTIs used in this study are also included. During the night (Fig. 2), the strength of the SBTI at a depth of $ID = 161$ m was 12.0 K (T_{hi} 16.4 °C − T_{h0} 4.4 °C). Thus, the vertical temperature gradient calculated based on the entire inversion layer (γ_i) reached + 7.5 K·100 m^{-1}. During the daytime (at 12 UTC), the temperature at the ground (2 m a.g.l.) during clear weather increased by 17.6 K, reaching 22.0 °C. The rate of temperature increase quickly decreased with altitude, and above 750 m, the daytime temperature was the same as that at night. Above the altitude of 250 m, the vertical temperature gradient was close to the dry adiabatic lapse rate (− 0.98 K·100 m^{-1}).

To assess the spatial extents of SBTIs, we calculated the percentage of SBTI co-occurring (regional SBTI), occurring only at one station (local SBTI) and percentage of days with no SBTIs at the stations, based on lapse rates for the 100-m near-ground layer (γ_{Sos}100 m, γ_{Wrc}100 m). The frequencies of SBTIs at midnight (00 UTC) and midday (12 UTC) were calculated for each month and each station to recognize their annual course.

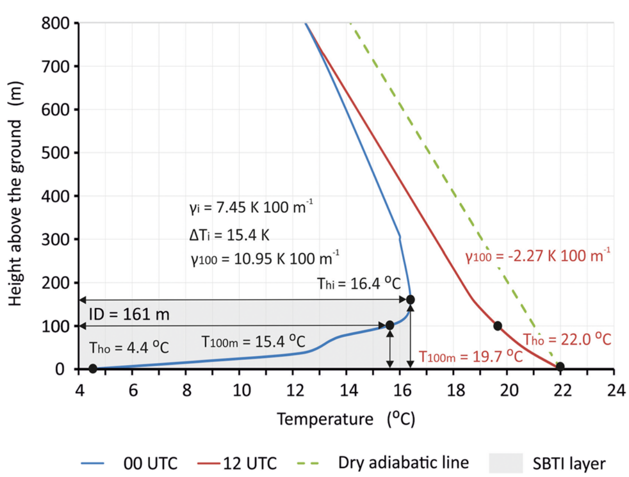

Fig. 2 Radiosonde temperature profiles in Wrocław on 9 April 2020 representing situations with a strong surface-based nocturnal inversion (00 UTC) and strong instability during the daytime (12 UTC)

To assess relationships between SBTIs and air pollutants, data on particulate matter PM_{10} in the GZM for the period from January 2001 to September 2020 for terms 00:00 and 12:00 UTC were selected. For these terms, representing midnight and midday conditions, the average values of PM_{10} and $PM_{2.5}$ concentrations were also calculated for individual months, seasons (winter, DJF; spring, MAM; summer, JJA; autumn, SON) and years (Jan–Dec). For PM_{10}, the regional mean was calculated as an average from 5 stations. In the case of Katowice, the concentrations of PM_{10} and $PM_{2.5}$ were considered, but the data on $PM_{2.5}$ existed for a shorter period (June 2009–September 2020). The average PM_{10} concentrations were also calculated for air stability classes to demonstrate the role of the SBTI in shaping the pollution level. Moreover, the concentration of pollutants was compared with the frequency of SBTI for each season.

3 Results and discussion

3.1 Comparison of the frequencies of the atmospheric stability classes in the lowest 100-m layer of the atmosphere in Sosnowiec and Wrocław

The frequencies of the air temperature gradients in the lowest 100-m layer of the atmosphere at midnight (00 UTC) were determined based on 6824 measurements in Sosnowiec (Table 2) and 7149 radiosonde soundings in Wrocław (Table 3). The annual frequency of nighttime SBTIs ($\gamma > 0.5$ K 100 m^{-1}) reached 47% in Sosnowiec and almost 59% in Wrocław, similar to Łeba (50%) located on the Baltic coast (Czarnecka et al. 2019) and Krakow (57% in 1972–1996 after Bokwa 2011) situated between the Vistula valley and the Carpathian Foothills. Lower frequency (by more than 10%) of the nocturnal SBTI in Sosnowiec than in Wrocław is connected with different physiographical factors. The frequency is usually higher in lowlands (Wrocław) and valleys (Kraków), than in uplands (Sosnowiec).

The data from the ERA-Interim reanalysis show that the frequency of SBTIs across most of Central Europe is 60% at 00 UTC (Palarz et al. 2018). Regional studies indicate a wide range of SBTI frequencies. For example, the frequency of nocturnal inversions in Athens was lower than that in Sosnowiec, reaching 44% (Katsoulis 1988). In Tehran, Iran, the annual frequency of boundary layer inversions in 2010–1014 was 62%, ranging from 54% in winter to 73% in summer (Tavousi and Abadi 2016). In the Bergen valley in Norway at night during winter in 2012/2013, SBTIs accounted for more than 60% of all measurements (Wolf et al. 2014). An extremely high frequency of temperature inversion was found over the Sichuan Basin in Southwest

Table 2 Seasonal and annual frequencies (in %) of the atmospheric stability classes in the lowest 100-m layer of the atmosphere in Sosnowiec (January 2001–September 2020) at 00 UTC

γ in K 100 m^{-1}	Stability and instability classes	Winter DJF	Spring MAM	Summer JJA	Autumn SON	Annual Jan–Dec
< -1.0	Strong instability	5.4	1.4	0.2	0.9	**2.0**
$\geq -1.0 \wedge < -0.5$	Conditional instability	32.4	15.3	7.9	15.6	**17.8**
$\geq -0.5 \wedge \leq 0.5$	Isothermal conditions	38.9	31.6	26.3	35.0	**32.9**
$> 0.5 \wedge < 1.0$	Weak inversion	5.5	6.6	9.3	5.8	**6.8**
$\geq 1.0 \wedge < 5.0$	Moderate inversion	14.2	32.9	45.1	30.7	**30.8**
≥ 5.0	Strong inversion	3.6	12.2	11.2	12.0	**9.7**
< -0.5	All instability	37.7	16.7	8.1	16.5	**19.8**
> 0.5	**All inversions**	**23.4**	**51.7**	**65.6**	**48.5**	**47.3**
n	Number of data	1717	1703	1739	1665	**6824**

Lack of data from 1 February 2001 to 19 October 2001

Data for all inversions an annual data are printed in bold

Table 3 Seasonal and annual frequencies (in %) of the atmospheric stability classes in the lowest 100-m layer of the atmosphere in Wrocław (January 2001–September 2020) at 00 UTC

γ in K 100 m^{-1}	Stability classes	Winter DJF	Spring MAM	Summer JJA	Autumn SON	Annual Jan–Dec
< -1.0	Strong instability	5.0	2.2	0.9	1.9	**2.5**
$\geq -1.0 \wedge < -0.5$	Conditional instability	27.6	17.1	7.2	17.4	**17.3**
$\geq -0.5 \wedge \leq 0.5$	Isothermal conditions	29.0	19.5	16.7	22.1	**21.6**
$> 0.5 \wedge < 1.0$	Weak inversion	8.2	8.3	9.4	7.9	**8.5**
$\geq 1.0 \wedge < 5.0$	Moderate inversion	24.3	34.8	44.4	33.2	**34.3**
≥ 5.0	Strong inversion	5.9	18.1	21.4	17.5	**15.8**
< -0.5	All instability	32.6	19.3	8.1	19.3	**19.8**
> 0.5	**All inversions**	**38.4**	**61.2**	**75.2**	**58.6**	**58.6**
n	Number of data	1765	1821	1817	1746	**7149**

Data for all inversions an annual data are printed in bold

China (Feng et al. 2020), where the annual and winter frequencies exceeded 74% and 95%, respectively.

Considering seasonal variability, SBTIs were rare in winter (23–38%) and frequent in summer (64–75%). Similar seasonal ranges of the SBTI frequency were recorded in Łeba (30 to 65%) and Prague (38% to more than 60%) (Stryhal et al. 2017; Czarnecka et al. 2019). This annual course of the SBTIs is typical over the predominant part of Europe (Palarz et al. 2018) and arises from a higher frequency of cloudless and calm nights in the summer than in winter. In spring, the frequency of SBTIs (52–61%) was higher than that in autumn (49–59%). The annual frequency of strong inversions ($\gamma \geq 5.0$ K 100 m^{-1}) was 10–16% and varied from 4–6% in winter to 12% in spring and autumn in Sosnowiec and up to 21% in summer in Wrocław.

Isothermal conditions ($\gamma \geq -0.5 \wedge \leq 0.5$ K 100 m^{-1}) were more common in Sosnowiec (33%) than in Wrocław (22%). Their frequency varied from 17–26% in summer to 29–39% in winter. In contrast, unstable conditions ($\gamma < -0.5$ K 100 m^{-1}) occurred during approximately 20% of the nights at both stations and varied from 8% in summer to 33–38% in winter.

The frequencies of air temperature gradients in the lowest 100-m layer of the atmosphere for midday (12 UTC) were determined based on 6827 measurements in Sosnowiec (Table 4) and 6429 radiosonde soundings in Wrocław (Table 5). At midday, SBTIs were very rare (0.6–0.7% of days a year). Their frequency increased to 1–2% only in winter. Similarly, low frequencies of midday inversions were characteristic of Prague (Stryhal et al. 2017), and the US Southern Great Plains area (ca. 0.3%) (Li et al. 2019). Daytime inversions occur more frequently on the Baltic coast in Łeba (8–9% in December and January) (Czarnecka et al. 2019). However, over most of Europe, the frequency of SBTIs does not exceed 2.5% (Palarz et al. 2018). Only in coastal zones and in the northern part of Europe does the frequency vary between 10 and 20%.

At midday, isothermal conditions were also infrequent, constituting 4–6% of days a year and peaking in winter (10–13% of days). The unstable conditions ($\gamma < -0.5$ K) prevailed on 93–95% of days a year. In winter, their frequency decreased to 86–88%. Summer was characterized by a high frequency (83–87%) of days with strong instability ($\gamma < -1.0$ K). The annual frequency of these days reached 69–71%, while in winter, it dropped to 40–53%.

Air temperature inversions mostly occur at night; therefore, in the next part of this paper, we focus on nocturnal SBTIs. The spatial extent of the SBTI was assessed by

Table 4 Seasonal and annual frequencies (in %) of the atmospheric stability classes in the lowest 100-m layer of the atmosphere in Sosnowiec (January 2001–September 2020) at 12 UTC

γ in K 100 m^{-1}	Stability classes	Winter DJF	Spring MAM	Summer JJA	Autumn SON	Annual Jan–Dec
< -1.0	Strong instability	53.4	81.9	83.2	66.1	**71.2**
$\geq -1.0 \wedge < -0.5$	Conditional instability	33.0	15.1	13.2	26.4	**21.9**
$\geq -0.5 \wedge \leq 0.5$	Isothermal conditions	12.0	2.8	3.1	7.1	**6.3**
$> 0.5 \wedge < 1.0$	Weak inversion	0.6	0.1	0.2	0.2	**0.3**
$\geq 1.0 \wedge < 5.0$	Moderate inversion	0.9	0.1	0.2	0.2	**0.3**
≥ 5.0	Strong inversion	0.1	0.0	0.1	0.0	**0.0**
< -0.5	All instability	86.4	97.0	96.4	92.5	**93.1**
> 0.5	**All inversions**	**1.6**	**0.2**	**0.5**	**0.4**	**0.6**
n	Number of data	1718	1704	1739	1666	**6827**

Lack of data from 1 February 2001 to 19 October 2001

Data for all inversions an annual data are printed in bold

Table 5 Seasonal and annual frequencies (in %) of the atmospheric stability classes in the lowest 100-m layer of the atmosphere in Wrocław (January 2003–September 2020) at 12 UTC

γ in K 100 m^{-1}	Stability classes	Winter DJF	Spring MAM	Summer JJA	Autumn SON	Annual Jan–Dec
< -1.0	Strong instability	40.0	83.2	87.3	64.4	**69.0**
$\geq -1.0 \wedge < -0.5$	Conditional instability	47.9	15.8	11.1	31.3	**26.3**
$\geq -0.5 \wedge \leq 0.5$	Isothermal conditions	10.1	0.8	1.3	3.8	**4.0**
$> 0.5 \wedge < 1.0$	Weak inversion	0.7	0.1	0.2	0.4	**0.3**
$\geq 1.0 \wedge < 5.0$	Moderate inversion	1.2	0.1	0.1	0.1	**0.4**
≥ 5.0	Strong inversion	0.1	0.0	0.0	0.0	**0.0**
< -0.5	All instability	87.9	99.0	98.4	95.7	**95.3**
> 0.5	**All inversions**	**2.0**	**0.2**	**0.3**	**0.5**	**0.7**
n	Number of data	1581	1641	1637	1570	**6429**

Data for all inversions an annual data are printed in bold its simultaneous occurrence in both the Silesian Upland (Sosnowiec) and Lower Silesian Lowland (Wrocław). The seasonal and annual frequencies of various combinations of SBTI occurrences are presented in Table 6. The symbol + in both the first and second columns means that SBTI occurred at both stations (regional inversions), while the symbol – means no inversion occurred at both stations. The SBTI is called local if it only occurs at one station. The regional SBTI constituted 40% of nights a year with a maximum of 57% in summer and 17% in winter.

The local SBTIs in Sosnowiec (no SBTI in Wroclaw) occurred during only 7% of the nights a year, with low seasonal variability from 6% in winter to 9% in summer. The local SBTIs in Wroclaw (no SBTI in Sosnowiec) were more frequent (19% of nights a year, 21% of winter nights). The total incidence of local SBTIs reached 26% and did not reveal apparent seasonal variability (25–27%). There were 34% of the nights per year without SBTIs at both stations. The frequency of nights without inversions revealed apparent seasonal variability, with a maximum in winter (56% of nights) and a minimum in summer (16% of nights).

The annual courses of local and regional SBTI frequency and days with no SBTI are presented in Fig. 3. The regional SBTI constituted more than 40% of nights from April to October, with a maximum in August (63%). In winter months, their frequency did not exceed 20%, dropping in January to 16%.

3.2 Annual course of the SBTIs

The nocturnal SBTIs have a clear annual course (Fig. 4). At both stations, the maximum frequency of SBTIs ($\gamma > 0.5$ K 100 m^{-1}) was found in August; however, in Sosnowiec, it was approximately 20% higher than in Wrocław (Sosnowiec: 64%, Wrocław; 80%). The lowest number of inversions was recorded in January and December (22–23% in Sosnowiec and 37–38% in Wrocław). The SBTI occurred with a frequency of more than 50% in the 6-month-long period between April and September in Sosnowiec and in the 8-month-long period between March and September in Wrocław. During these months, the SBTI frequency in Wrocław was higher by ca. 15% than in Sosnowiec. In Sosnowiec, the strongest SBTI ($\gamma \geq 5.0$ K 100 m^{-1}) appeared during a minimum of 3% in December to 16% of nights in September. In Wrocław, the highest frequency of strongest inversions was found in July (25%).

Table 6 The seasonal and annual frequencies (%) of regional (SBTI at both stations) and local (SBTI at one station) SBTI and nights with no SBTI in the lowest 100 m near the ground layer of the atmosphere (Jan 2001–Sep 2020) at midnight (00 UTC)

SBTI Sosnowiec $\gamma > 0.5$ K 100 m^{-1}	SBTI Wrocław $\gamma > 0.5$ K 100 m^{-1}	Winter DJF	Spring MAM	Summer JJA	Autumn SON	Annual Jan–Dec
+	+	17.4	44.8	57.0	40.8	**40.0**
+	–	5.9	7.1	8.5	7.8	**7.3**
–	+	21.1	17.7	18.9	17.8	**18.9**
–	–	55.6	30.4	15.6	33.6	**33.8**
n	Number of cases	1708	1686	1732	1654	**6780**

Explanations two first columns: + SBTI exist; – without SBTI

Annual data are printed in bold

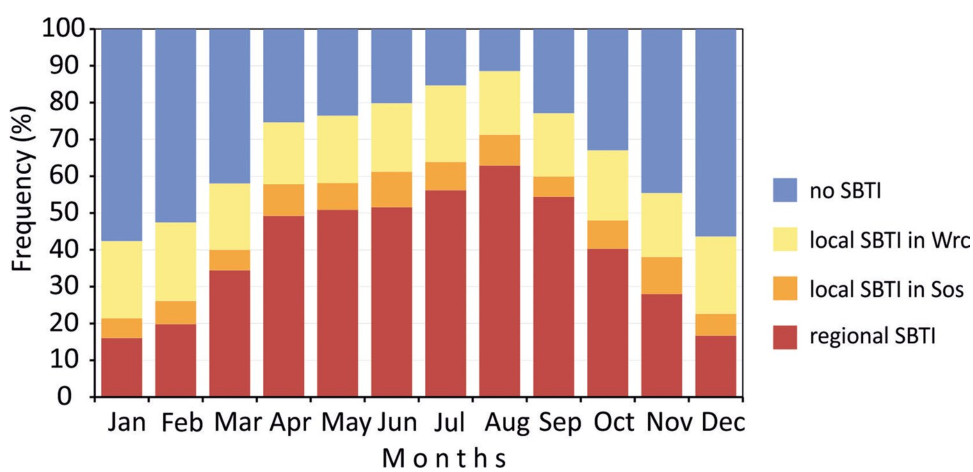

Fig. 3 Comparison of the annual course of the common structure of the vertical lapse rate of air temperature in the lowest 100 m near the ground layer between Sosnowiec and Wrocław (Jan 2001–Sep 2020) at midnight (00 UTC)

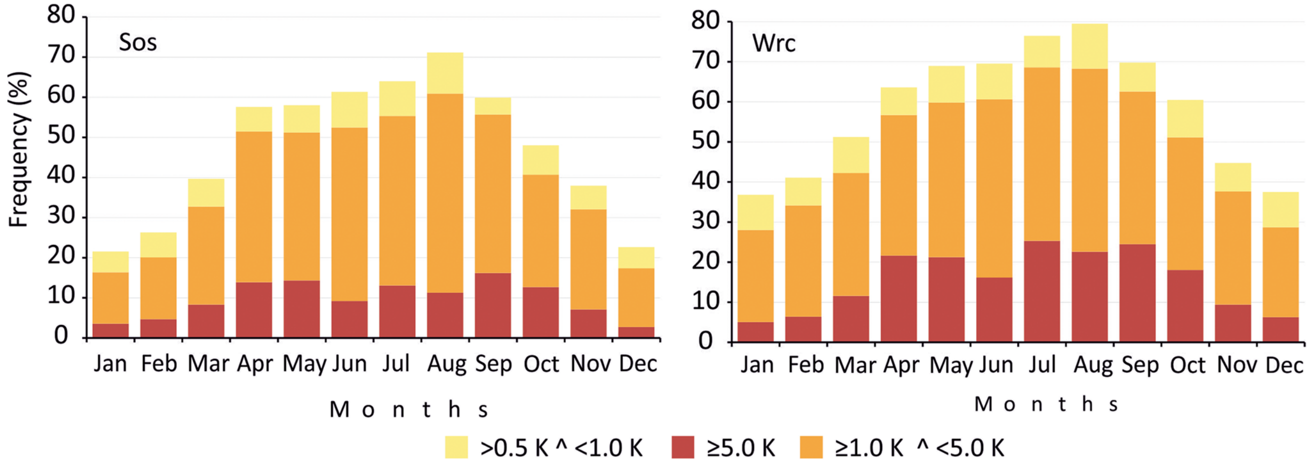

Fig. 4 Annual course of the surface-based air temperature inversions (SBTI) in Sosnowiec (Sos) and Wrocław (Wrc) from January 2001–September 2020 at 00 UTC with respect to the SBTI gradient (γ at K·100 m^{-1})

3.3 Depth and strength of the surface-based inversions of temperature (SBTI) in Wrocław

The vertical measurements at only two points, as in Sosnowiec, did not allow the height of the inversion layer to be assessed. Therefore, this characteristic was investigated based on soundings from Wrocław. Due to the similar intra-annual pattern of the SBTI frequency at both stations, we assume that Wrocław can also represent the general pattern of the SBTI depth in Sosnowiec. The Europe-wide study of SBTIs by Palarz et al. (2018) also indicates similarity in the characteristics of SBTIs over central Europe.

The deepest SBTI in Wrocław reached a height of 1561 m (Table 7) and a strength of 17.1 K. Five inversions were as deep as 1250 m. They occurred in the winter months and in November during anticyclonic situations with weakened polar continental air advection (Pc) or during advection of polar maritime warm air (Pmw) from the southwestern sector. The SBTI strength (ΔT_{i}) reached 6–19 K and showed no dependence on the inversion layer depth (ID). In Łeba (Czarnecka et al. 2019), the maximum thickness of the nocturnal SBTIs was recorded in January (1632 m) and July (1397 m).

The vertical distribution of air temperature in Wrocław up to 3000 m above ground level for 2 days with a very thick and exceptionally strong SBTI (ΔT_{i} 17–19 K) is shown in Fig. 5A. During midday (12 UTC), the SBTI disappeared only in the near-ground level of the atmosphere due to insolation. During the first day, the SBTI disappeared up to approximately 250 m, and on the second day, it disappeared to 600 m. However, the elevated inversion reaching an altitude of 1000–1200 m remained. At night on 4 November 2015, the air temperature at the ground (2 m) dropped to − 2.1 °C again, while at an altitude of 1561 m, it was + 15.0 °C. At midday on 4 November, at 12.00 UTC, the inversion base was elevated to 600 m with its depth and strength reaching 600 m and 4.6 K, respectively.

The strongest SBTI (ΔT_{i} 20.1–20.9 K) appeared at midnight on the 13th and 14th of January 2009 (Table 8).

Table 7 Characteristics of the five thickest SBTIs in Wrocław at 00 UTC (Jan 2001–Sep 2020)

Date	Circulation type	Air mass	ID m	ΔT_{i}	γ_{i}	γ_{Wrc}100 m	γ_{Sos}100 m
Nov 4, 2015	Ka	Pc	1561	17.1	1.1	10.8	9.3
Jan 9, 2017	Ka	Pc	1388	6.0	0.4	4.2	8.9
Feb 4, 2014	Sa	Pmw	1346	9.4	0.7	2.2	1.4
Dec 14, 2013	Wa	Pmw	1313	10.3	0.8	4.7	2.1
Nov 3, 2015	SWa	Pc	1254	19.1	1.5	11.5	8.2

Explanations: ΔT_i, inversion strength or intensity in K; γ_i, average vertical lapse rate for the whole SBTI layer (ID) in K 100 m^{-1}; γ_{Wrc}*100 m*, γ_{Sos}*100 m*, lapse rate for the lowest 100 m in Wrocław and in Sosnowiec. Circulation types: *Ka*, anticyclonic wedge; *Wa, Sa, SWa*, anticyclonic situations with air advection from W, S and SW. Air mass: *Pc*, polar continental air; *Pmw*, polar maritime warm air (description of circulation types and air masses is given in Sect. 2.2)

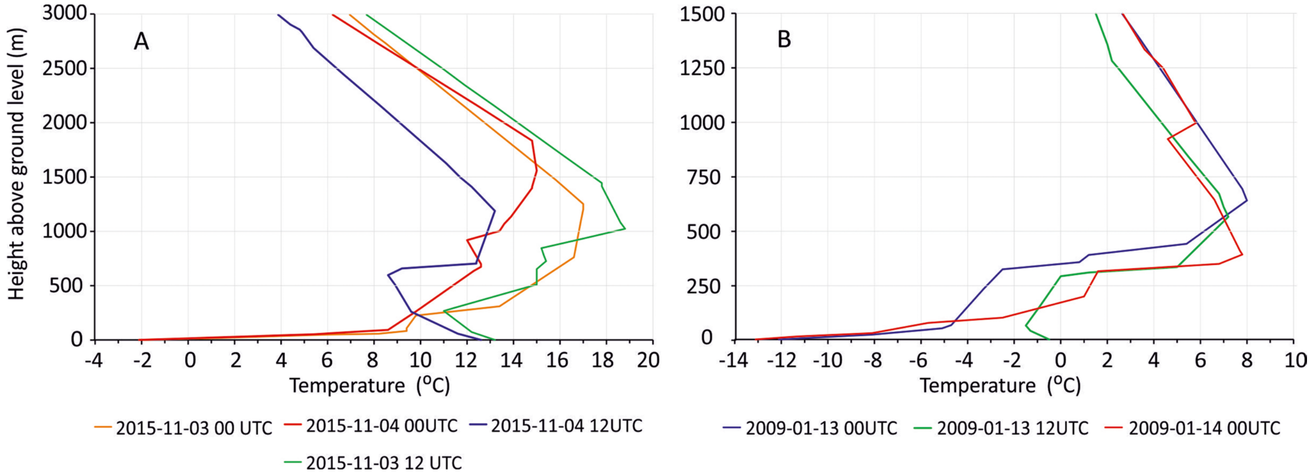

Fig. 5 Example of the thickest (**A**) SBTIs on 3 and 4 November 2015 ($ID=1254$ and 1561 m) and the strongest (**B**) SBTIs on 13 and 14 January 2009 in Wrocław. For comparison, the vertical profiles of temperature during midday are also presented

Table 8 Characteristics of the five strongest SBTIs in Wrocław at 00 UTC (Jan 2001–Sep 2020)

Date	Circulation type	Air mass	ΔT_i	ID m	γ_i	γ_{Wrc}100 m	γ_{Sos}100 m
14 Jan 2009	Ka	Pc	20.9	391	5.4	10.6	1.0
13 Jan 2009	Wa	Pc	20.1	640	3.1	7.7	2.8
3 Nov 2015	SWa	Pc	19.1	1254	1.5	11.5	8.2
12 Jan 2009	Wa	Pc	17.3	834	2.1	8.2	1.6
4 Nov 2015	Ka	Pc	17.1	1561	1.1	10.8	9.3

Explanations: as at Table 7

The depths of these inversion layers were 640 and 391 m, respectively. In the near-ground 100-m layer of the troposphere, the lapse rate (γ_{Wrc}100 m) was exceptionally high, exceeding 10 K 100 m^{-1}. The vertical profile of air temperature for these SBTIs is presented in Fig. 5B. At midday on 13 January 2009, the temperature inversion disappeared only in the near-ground 64-m-thick layer. Above this height, the elevated inversion with a thickness of 490 m and a strength (ΔT_i) of 8.7 K still existed. During these inversions, the synoptic conditions were similar to the deepest SBTIs on 4 November 2015 (described above).

The statistical distribution of the depth (ID) of nocturnal SBTIs ($\Delta T_i > 0.5$ K) in Wrocław calculated from a large number of cases (4559) is presented in Table 9. The average annual ID equal 207 m and vary from 186 m in spring to 249 m in winter. In spring, mean SBTI depths range from 100–150 m over Western Europe and increase to 150–200 m above the central and eastern parts of the continent (Palarz et al. 2018). Even higher SBTI depths, exceeding 200 m, were found in winter in Central and Eastern Europe and Scandinavia. In the Bergen Valley, Norway, the mean inversion top is located at 220 m a.s.l. (Wolf et al. 2014). In the Southern Great Plains in the USA, the mean SBTI depth is slightly shallow, reaching 198 m (Li et al. 2019). In Łeba (Czarnecka et al. 2019) in 2005–2014, the mean thickness of the nighttime inversions varied from 143 m in December to 218 m in April.

Table 9 Statistical characteristics of the SBTI depth (ID in m) in Wrocław at 00 UTC (Jan 2001–Sep 2020)

Percentiles and other elements	Winter DJF	Spring MAM	Summer JJA	Autumn SON	Annual Jan–Dec
Max	1388	749	741	1561	**1561**
$p=99\%$	1058	532	514	754	**740**
$p=95\%$	677	350	364	466	**447**
$p=90\%$	538	302	308	378	**344**
$p=75\%$	309	233	233	262	**246**
$p=50\%$	**175**	**174**	**173**	**191**	**178**
$p=25\%$	114	122	131	135	**127**
$p=10\%$	67	79	95	99	**87**
$p=5\%$	46	58	77	70	**65**
$p=1\%$	22	33	35	41	**33**
Min	8	17	17	16	**8**
Average	**249**	**186**	**192**	**221**	**207**
n of data	772	1213	1458	1116	**4559**

Data averages, median and annual data are printed in bold

Table 10 Seasonal and annual depth (ID) of the surface-based temperature inversion layer frequency (in %) in Wrocław at 00 UTC (Jan 2001–Sep 2020)

ID in m	Winter DJF	Spring MAM	Summer JJA	Autumn SON	Annual Jan–Dec
0–50	7.1	3.7	2.1	2.6	**3.5**
50–100	12.7	12.6	9.8	8.2	**10.7**
100–150	**21.1**	22.1	24.3	21.7	**22.5**
150–200	16.7	**24.0**	**26.9**	**22.6**	**23.3**
200–250	9.8	17.1	17.6	17.1	**16.0**
250–300	6.5	10.2	8.3	9.6	**8.8**
300–350	4.8	5.3	5.4	6.7	**5.6**
350–400	3.8	2.3	2.3	3.2	**2.8**
400–450	2.7	1.3	1.2	2.9	**1.9**
450–500	3.0	0.1	0.9	1.2	**1.1**
500–550	2.2	0.5	0.5	0.9	**0.9**
550–600	1.7	0.3	0.3	0.4	**0.6**
600–650	2.1	0.2	0.2	0.8	**0.7**
650–700	0.9	0.2	0.1	0.4	**0.3**
> 700	4.9	0.1	0.1	1.7	**1.3**
***n* of data**	**772**	**1213**	**1458**	**1116**	**4559**
50–250	60.3	75.8	78.6	69.6	72.5
50–300	66.8	86.0	86.9	79.2	81.3
100–250	47.6	63.2	68.8	61.4	61.8

The ID with the highest frequency of inversion, maximum frequency of inversions, annual data and number of data are printed in bold

In Athens, on the other hand, in 1971–1983, the SBTI depth ranged from 140 m in December to 270 m in August (Katsoulis 1988); however, the data for the more extended period 1974–2001 (Kassomenos and Koletsis 2005) indicated depths from 169 m in summer, 172 m in winter and 190 m in transient seasons.

Similar results (175 to 198 m) were reported from Hemsby (UK) based on radiosonde data for the 1976–1980 period (Milionis and Davies 2008). The deepest SBTIs, reaching an average of 212 m, were found over the Sichuan Basin in China (Feng et al. 2020) Please confirm that this is correct."-->, with seasonal variability from 177 m in winter to 257 m in summer. Such a seasonal distribution differs from that in Wrocław, where the highest depths were recorded in autumn (1561 m on 4 November 2015) and in winter (1388 m on 9 January 2017). However, in summer and spring, they did not exceed 750 m (Table 9). The threshold depths corresponding to quartiles ($p = 25\%$ and 75%) that encompass 50% of the sampling ranged from 127 to 246 m for a year. In winter, the quartile range was the largest (114–309 m). In summer, it ranged from 131 to 233 m. There was a 10% probability of SBTIs with a thickness exceeding 538 m in winter and a 5% probability that the ID was larger than 677 m.

The frequencies of SBTI depths within 50-m-wide ID ranges are shown in Table 10 and Fig. 6. In spring and

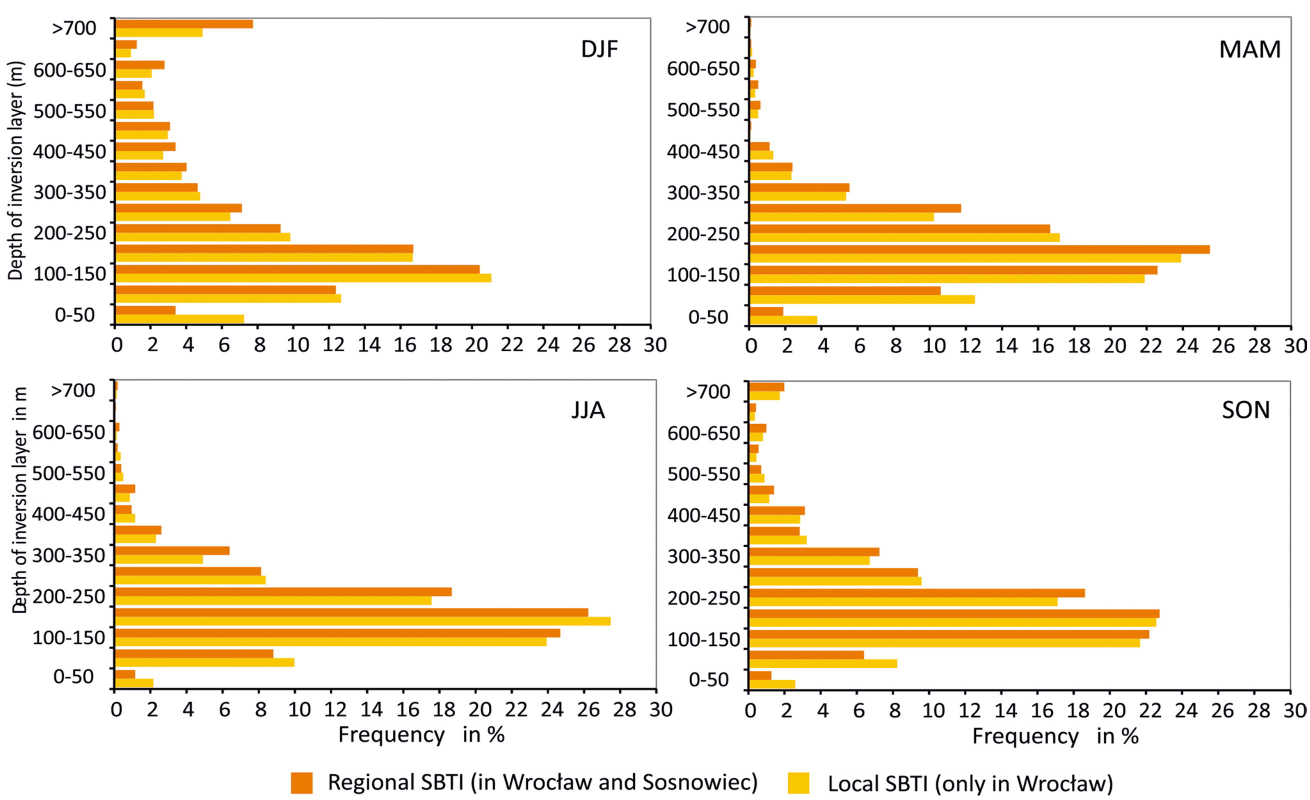

Fig. 6 Seasonal frequency of the midnight SBTI layer depth (ID in m) in Wrocław. DJF, winter; MAM, spring; JJA, summer; SON, autumn

summer, IDs exceeding 700 m were very rare (0.1%). Their annual frequency was 1.3% and varied seasonally between 1.7% in autumn and 4.9% in winter. In winter, the most frequent ID (21%) was within the range of 100–150 m. In other seasons and on an annual scale, the SBTI depth most often ranged between 150 and 200 m (23.3% in the year with a maximum in summer of 26.8%).

The ID frequency jointly for the ranges between 100 and 250 m reached 61.9% on an annual scale and 68.7% in summer. In winter, when the ID distribution was most flattened, SBTIs of 100–250-m depth constituted the minimum of 47.7% of all cases. Annually, the majority of SBTI depths fell within 50–300 m (81% ranging from almost 67% in winter to 87% in summer).

Histograms of the ID frequencies for individual seasons, calculated for regional inversions occurring simultaneously at both stations ($n = 2851$) and local inversions in Wrocław ($n = 4559$), are presented in Fig. 6. The distributions of regional and local IDs were very similar, as evidenced by minor frequency differences in particular ranges. However, the depths of regional SBTIs were slightly thicker than those of local SBTIs. The ID frequencies for regional SBTIs were usually somewhat larger in deeper classes and lower in shallower classes compared to regional SBTIs.

Table 11 Coefficients of correlation (r) and determination (r^2*100 in %) between depth of the SBTI (ID) at 00 UTC in Wrocław and inversion strength (ΔT_i), as well as the vertical temperature gradient (γ_i) across the whole inversion layer

Season	Number of data n	ΔT_i		γ_i	
Coefficients		r	r^2*100	r	r^2*100
DJF	323	0.54	29	−0.41	17
MAM	792	*0.03*	*0*	−0.49	24
JJA	1033	*−0.01*	*0*	−0.52	27
SON	703	0.38	14	−0.42	17

$r > 0.32$ are significant at the level $\alpha = 0.001$

3.4 Correlations between the characteristics of SBTI

In this section, the SBTI strength in the 100-m near-ground layer and depth was correlated with other characteristics of the vertical structure of the SBTIs (Tables 11 and 12) to check whether and which indirect information can be drawn based on the data from the 100-m near-ground layer. The basic characteristics of the SBTIs, including its strength (ΔT_i) and depth, were significantly correlated ($\alpha = 0.01$) only in winter ($r = 0.54$) and autumn ($r = 0.38$), which means that strong inversions were deeper than weaker SBTIs (percentage of explained variability (r^2*100): 54% and 38%). On the other hand, the vertical temperature gradient (γ_i) across the entire inversion layer was significantly but negatively correlated with ID in each season, with the highest percentage of explained variance in autumn. In other seasons, the percentage of explained variance was lower: 24% in spring and 17% in winter and autumn. The negative relations mean that the thicker the inversion layer was, the smaller the average temperature gradient for that layer.

The inversion strength (ΔT_i) showed a positive correlation with the vertical temperature gradient (γ_i) across the whole inversion (Table 11), especially in summer and spring (coefficient of determination r^2*100 = 51–54%). Only in winter was the correlation coefficient low; however, it was still significant at 0.31 (r^2*100 = 10%). This index (ΔT_i) was the strongest correlated with the temperature gradient in the lowest 100-m near-ground air layer (γ_{Wrc}100 m) (Table 12). The strength of the SBTI was also significantly related to the average lapse rate for the lower layer of the atmosphere from the ground surface to the isobaric level of 850 hPa (γ_{850}) at an altitude of approximately 1500 m above sea level. In this case, the correlation coefficients ranged from 0.71 in autumn to 0.80 in winter (51–64% explained variance).

Table 12 Coefficients of correlation (r) and determination (r^2*100 in %) between the SBTI strength (ΔT_i) and vertical temperature gradient (γ_i) across the whole inversion layer, lapse rate for the lowest atmosphere layer up to 850 hPa level (γ_{850}) and lapse rate for the 100 m near the ground layer (γ_{Wrc}100 m) at 00 UTC in Wrocław

Season	γ_i		γ_{850}		γ_{Wrc}100 m	
Coefficients	r	r^2*100	r	r^2*100	r	r^2*100
DJF	0.31	10	0.80	64	0.74	55
MAM	0.71	51	0.75	56	0.93	86
JJA	0.73	54	0.79	63	0.90	82
SON	0.54	29	0.71	51	0.88	77

$r > 0.32$ are significant at the level $\alpha = 0.001$

Table 13 Comparison of the six strongest SBTIs at the lowest 100 m in Sosnowiec in comparison with particular SBTIs in Wrocław at 00 UTC (Jan 2001–Sep 2020)

Date	Circulation type	Airmass	γ_{Sos}100 m	γ_{Wrc}100 m	ID m	ΔT_i	γ_i
9 Apr 2020	Ka	Pc	12.5	11.0	161	12.0	7.5
25 Oct 2019	Wa	Pmo	11.9	7.2	162	10.8	6.7
1 May 2012	Ka	T	10.5	5.0	273	8.2	3.0
24 Dec 2010	Sc	T	10.4	0.7	462	11.1	2.4
13 May 2008	X	Pmo/A	9.7	7.8	213	9.8	4.6
4 Feb 2002	Wa	Pmw	9.4	5.1	76	5.2	6.8

Explanations: as at Table 7 and Sc, cyclonic situation with air advection from S; X, baric col; Pmo, polar maritime old air; A, arctic air; T, tropical air

Table 14 Comparison of the six strongest SBTIs at the lowest 100 m in Wrocław in comparison with Sosnowiec and other SBTI characteristics in Wrocław at 00 UTC (Jan 2001–Sep 2020)

Date	Circulation type	Airmass	γ_{Wrc}100 m	γ_{Sos}100 m	ID m	ΔT_i	γ_i
19 Mar 2010	Wa	Pmw	12.9	2.8	329	14.4	4.4
21 Apr 2019	Ka	Pc	11.6	5.5	104	11.6	11.2
3 Nov 2015	SWa	Pc	11.5	8.2	1254	19.1	1.5
5 Jul. 2015	SWa	Pmw	11.5	5.4	150	12.0	8.0
5 Dec 2010	SWa	Pc	11.0	−0.2	613	15.0	2.4
9 Apr 2020	Ka	Pc	11.0	12.5	161	12.0	7.4

Explanations: as at Table 7

3.5 Lapse rates and weather conditions for the strongest local SBTI—comparison between the stations

In this section, we selected the strongest SBTI in Sosnowiec (6 cases, Table 13) and in Wrocław (6 cases, Table 14) and compared the lapse rates and weather conditions for that day at the stations. Interestingly, only one of these SBTIs (9 April 2020) was regional and occurred simultaneously at both stations. The highest values of γ_{Sos}100 m in Sosnowiec ranged from 9.4 to 12.5 K·100 m^{-1}. At the same time, in Wrocław, the gradients were smaller (from 5.0 to 11.0 K·100 m^{-1}). Most of these SBTIs occurred in anticyclonic synoptic situations.

The situation on 24 December 2010 was unusual due to a large difference in gradients between the stations: 10.4 K 100 m^{-1} (Sosnowiec) and 0.7 K 100 m^{-1} (Wrocław). Such a difference was caused by a weather front located between the stations separating the tropical air mass (T) flowing in from the south to Sosnowiec and the old cooler polar maritime air mass (Pmo) flowing from the NE into Wrocław. In Wrocław, there was fog at the ground layer with a small temperature gradient. In the 100-m layer, the temperature increased from − 2.5 to − 1.8 °C at an altitude of 100 m. Above that level, there was a very rapid increase in air temperature that reached + 7 °C at an altitude of 200 m. The temperature increased further to + 8.6 °C at a height of 462 m. Thus, the strength of the inversion ΔT_i reached 11.1 K.

Table 14 includes the strongest SBTI in Wrocław and compares them with the data from Sosnowiec for the same days. The γ_{Wrc}100-m lapse rates ranged from 11.0 to 12.9 K 100 m^{-1}. In Sosnowiec, the air temperature gradients on those days were much smaller (from 2.8 to 8.2 K 100 m^{-1}). The SBTI on 9 April 2020 was exceptional due to the large gradient that was also found in Sosnowiec (12.5 K 100 m^{-1}). Interestingly, despite many similarities, there were often large differences between the two studied regions in extreme cases. They were caused either by a differing synoptic situation (compare the example described above with 24 December 2010) or local weather conditions. The SBTI and weather conditions on 5 December 2020 can serve as an interesting example. On that night (00 UTC), both stations were under the influence of anticyclonic situations with air advection from the SW. In Wrocław, the temperature gradient in the ground layer (γ_{Wrc}100 m) was as high as 11.0 K 100 m^{-1}. In Sosnowiec, the SBTI appeared earlier during cloudless and frosty conditions at 21 UTC (γ_{Sos}100 m = 5.2 K 100 m^{-1}). However, from 23 UTC, a radiation fog formed with a thickness exceeding 100 m, which led to a near-isothermal distribution of temperature in this layer. There is a high probability that the upper/elevated temperature inversion above the fog layer persisted, which was suggested by the large ID in Wrocław amounting to 613 m.

The vertical profile of air temperature up to a height of 1000 m above the ground in Wrocław is shown in Fig. 7 for the nocturnal strongest SBTI on 19 March 2010. The strength of the inversion (ΔT_i) with a thickness of 329 m was

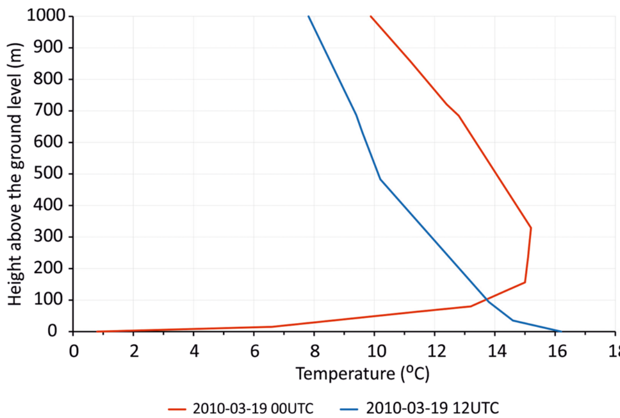

Fig. 7 Example of the midnight SBTI in Wrocław with the strongest gradient in the lowest 100-m layer during 19 March 2010 (γ_{Wrc}100m = 12.9 K 100 m^{-1}). For comparison, the vertical profile of temperature during midday is also presented

14.4 K. At midday (12 UTC), the SBTI disappeared within the entire profile due to the effect of solar radiation. Above 100 m, the air temperature was reduced by approximately 3–4 K.

To determine the detailed characteristics of the strongest SBTI in Sosnowiec where no soundings exist, correlations were calculated between the gradient in the 100-m near-ground layer (γ_{Sos}100 m) and the SBTI characteristics in Wrocław. It allowed assessing the degree of representativeness of the SBTI in Sosnowiec for a larger area of southern Poland. No relations were found between γ_{Sos}100 m and the inversion layer thickness in Wrocław (ID). No such relationship was found between these characteristics (γ_{Wrc}100 m and ID) in Wrocław.

On the other hand, the air temperature gradient in Sosnowiec (γ_{Sos}100 m) showed significant relations at the level of $\alpha = 0.01$ (Table 15) with comparable data for Wrocław (γ_{Wrc}100 m). The percentage of explained variance reached its maximum of 23% in spring. Slightly stronger relationships explaining 25% of the variance were found between the average temperature gradient for the entire inversion layer (γ_{i}). Weaker, although statistically significant, were the relationships between γ_{Sos}100 m and temperature gradients in the layer up to 1500 m (isobaric level 850 hPa) in Wrocław. This relationship was stable all year round ($r = 0.34$–0.37; r^2*100 = 12–14%).

3.6 *Impact of SBTIs on air pollution (PM_{10} and $PM_{2.5}$)*

Temperature inversions contribute to a high concentration of air pollution in this layer. This is particularly true in the case of SBTIs that are formed in winter at low temperatures. Such an episode of high pollution occurred on 9 January 2017, when, in a high-pressure situation (anticyclonic wedge) in a polar continental air mass, the air temperature in Sosnowiec at the ground dropped to − 19.2 °C. Then, an SBTI occurred, and at a height of 88 m above the ground, the air

Table 15 Coefficients of correlation (r) and determination (r^2*100 in %) between lapse rate for the 100 m near the ground layer (γ_{Sos}100 m) during SBTI at 00 UTC in Sosnowiec, with other SBTI characteristics in Wrocław

Season	γ_{i} Wrocław		γ_{850} Wrocław		γ_{Wrc}100 m	
Coefficients	r	r^2*100	r	r^2*100	r	r^2*100
DJF	0.27	7	0.34	12	0.29	8
MAM	0.50	25	0.35	12	0.48	23
JJA	0.43	18	0.36	13	0.40	16
SON	0.44	19	0.37	14	0.43	18

$r > 0.32$ are significant at the level $\alpha = 0.001$

Table 16 Comparison of the winter maximum PM_{10} concentration (max PM_{10} in µg·m^{-3}) in the Upper Silesia Region with SBTI characteristics in Sosnowiec and Wrocław at 00 UTC (Jan 2001–Sep 2020)

Station	Date	Max PM_{10}	Circulation type	Air mass	γ_{Sos}100 m K·100 m^{-1}	γ_{Wrc}100 m K·100 m^{-1}	ID m	ΔT_{i} K	γ_{i} K·100 m^{-1}
Dąbrowa Górnicza PM_{10}	29 Jan 2006	522	Ka	Pc	9.4	10.3	190	12.0	6.3
Sosnowiec PM_{10}	13 Feb 2012	772	Ka	Pmo	4.9	6.8	226	7.8	3.4
Zabrze PM_{10}	10 Jan 2017	1159	SWa	Pc	2.4	*− 0.6*	-	-	-
Gliwice PM_{10}	4 Jan 2002	799	Ca	A	4.4	4.7	162	5.2	3.2
Katowice PM_{10}	10 Jan 2017	516	SWa	Pc	2.4	*− 0.6*	-	-	-
Katowice $PM_{2.5}$	27 Jan 2010	641	Ka	Pc	2.6	6.9	325	12.0	3.7
Average PM_{10} from 5 stations	10 Jan 2017	634	SWa	Pc	2.4	*− 0.6*	-	-	-

Explanations: as at Tables 7 and 13 (*Ca*, centre of anticyclone). Italicized numbers are for the negative gradients (lack of inversion). Data for Katowice $PM_{2.5}$ are from the shorter period Jun 2009–Sep 2020

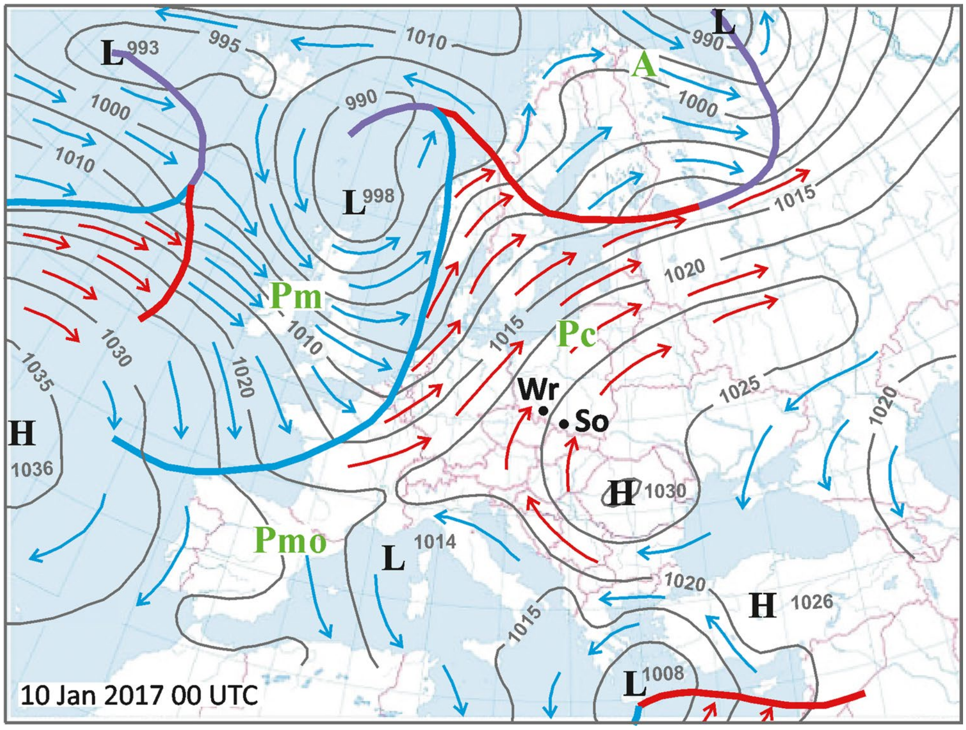

Fig. 8 Synoptic map of Europe 10 Jan 2017 (00 UTC) with SWa circulation typical for the highest PM_{10} concentration in Zabrze. Isobars and atmospheric fronts (blue, cold; red, warm; violet, occlusion) were taken from the synoptic map of the German Meteorological Service (www.wetter3.de/archiv_dwd.html). The arrows indicate the direction of the geostrophic wind in the advection of warm (red) and cool (blue) air. Explanations: L, low centre; H, high centre. Air mass: A, arctic; Pc, polar continental; Pm, polar maritime; Pmo, polar maritime old; So, Sosnowiec; Wr, Wrocław

temperature was −11.5 °C, and the vertical gradient (γ_{Sos}100 m) reached +8.94 K 100 m^{-1}. During that night, the hourly PM_{10} concentration reached 985 μg·m^{-3} in Dąbrowa Górnicza and 945 μg·m^{-3} in Zabrze. In Katowice, at 04 UTC, the PM_{10} concentration was 667 μg·m^{-3}, and the $PM_{2.5}$ concentration was 600 μg·m^{-3}.

This situation with a high PM_{10} concentration maintained by the SBTI lasted for 5 days (7–11 January 2017). The highest PM_{10} concentration amounted to 1159 μg·m^{-3} in Zabrze (Table 16) and occurred on 10 January 2017. On that day, the region was under the influence of an anticyclonic situation (Fig. 8) with air advection from the SW (SWa). The highest concentration of PM_{10} was also recorded in Katowice (516 μg·m^{-3}) and generally in Upper Silesia (average from 5 stations: 624 μg·m^{-3}). The concentration of $PM_{2.5}$ in Katowice was also high (417 μg·m^{-3}). On that day, the nocturnal SBTI (10 January 2017) was maintained only in Upper Silesia, while in Wrocław, a negative air temperature gradient was recorded in the near-ground 100-m atmospheric layer (γ_{Wrc}100 m = −0.6 K 100 m^{-1}).

The highest concentration of $PM_{2.5}$ in Katowice (641 μg·m^{-3}) was recorded on 27 January 2010, in the mass of polar continental air (Pc) under the influence of an anticyclonic wedge (Ka). The air temperature gradients at 100-m near-ground level reached +2.4 K 100 m^{-1} in Sosnowiec and +6.9 K 100 m^{-1} in Wrocław. The inversion was 325-m deep, and its strength (ΔT_i) amounted to 12.0 K.

Another episode of exceptionally strong winter SBTIs in southern Poland occurred from 25–30 January 2006. On 29 January 2006 (Table 16), the air temperature gradients reached as much as 9.4 K 100 m^{-1} in Sosnowiec and 10.3 K 100 m^{-1} in Wrocław. The inversion was 190-m deep in the near-ground layer. At 00 UTC in Dąbrowa Górnicza, the PM_{10} concentration reached 522 μg·m^{-3}, which was the highest concentration during the entire measurement period in that city. A very high concentration on that day was also recorded in Zabrze (916 μg·m^{-3}). During this episode (25–30 January 2006), high concentrations of PM_{10} also occurred in Sosnowiec (515–614 μg·m^{-3}) and Katowice (383–473 μg·m^{-3}). On 25 January 2006, in Wrocław, a very strong inversion formed (ΔT_i) with a gradient of 15.4 K and a depth of 472 m. At that time, vertical air temperature gradients in the ground layer were also very high in Wrocław (γ_{Wrc}100 m = 9.4 K 100 m^{-1}) and in Sosnowiec (γ_{Sos}100 m = 5.1 K 100 m^{-1}).

The highest concentrations of PM_{10} in Sosnowiec (772 μg·m^{-3}) on 13 February 2017, and in Gliwice (799 μg·m^{-3}) on 4 January 2002, were accompanied by the presence of SBTIs (Table 16). During these episodes of high concentration of air pollution, the vertical temperature gradients in Sosnowiec (γ_{Sos}100 m) ranged from 4.2–5.8 K·100 m^{-1} (11–13 February 2012) and 2.3–4.6 K·100 m^{-1} (4–6 January 2002). The strong influence of SBTIs on the high concentration of PM_{10} during the winter season was also found in selected cities located in the Polish Carpathians (Palarz et al. 2015; Palarz and Celiński-Mysław 2017). During the strongest episode of pollution from 23 January to 2 February 2006, the maximum

Table 17 Comparison of the spring maximum PM_{10} concentration (Max PM_{10} in $\mu g \cdot m^{-3}$) in the Upper Silesia Region with SBTI characteristics in Sosnowiec and Wrocław at 00 UTC (Jan 2001–Sep 2020)

Station	Date	Max PM_{10}	Circulation type	Air mass	γ_{Sos}100 m K·100 m^{-1}	γ_{Wrc}100 m K·100 m^{-1}	ID m	ΔT_i K	γ_i K·100 m^{-1}
Dąbrowa Górnicza PM_{10}	5 Mar 2011	357	NWa	Pc	1.6	4.57	140	4.9	3.5
Sosnowiec PM_{10}	22 Mar 2011	376	NWa	Pmo	5.9	7.1	198	7.9	4.0
Zabrze PM_{10}	22 Mar 2011	564	NWa	Pmo	5.9	7.1	198	7.9	4.0
Gliwice PM_{10}	4 Mar 2011	396	Ka	Pc	4.2	5.5	180	6.5	3.6
Katowice PM_{10}	4 Apr 2018	329	SWc	Pmw	7.3	3.1	206	4.2	2.0
Katowice $PM_{2.5}$	8 Mar 2015	206	SWa	Pmw	2.1	4.8	197	5.6	2.8
Average PM_{10} from 5 stations	22 Mar 2011	327	NWa	Pmo	5.9	7.1	198	7.9	4.0

Explanations: as in Tables 7 and 13. Data for Katowice $PM_{2.5}$ are from the shorter period Jun 2009–Sep 2020

concentration of PM_{10} was recorded on 29 January 2006, in Nowy Sącz (500 $\mu g \cdot m^{-3}$) and Żywiec (505 $\mu g \cdot m^{-3}$), similar to that recorded in Dąbrowa Górnicza (see Table 16). Additionally, in Wrocław, the maximum daily concentrations of PM_{10} (Kamińska 2017) on 12 February 2017, and 15 February 2017, occurred with strong temperature inversions ($ID = 266$ m, $\Delta T_i = 8.4$ K, $\gamma_{Wrc}100\ m = 7.0$ K 100 m^{-1}; $ID = 935$ m, $\Delta T_i = 12.5$ K, $\gamma_{Wrc}100\ m = 5.6$ K 100 m^{-1}).

In spring (MAM), the maximum PM_{10} concentrations at night (00 UTC) were lower (Table 17) than those in winter. The highest concentrations were recorded on 22 March 2011, in Zabrze (564 $\mu g \cdot m^{-3}$) and Sosnowiec (376 $\mu g \cdot m^{-3}$). In Upper Silesia, the average concentration equalled 327 $\mu g \cdot m^{-3}$, and it was the spring maximum during the research period. During this episode, the weakening anticyclonic wedge transformed into the NWa situation with the influx of polar maritime old air masses. On the night of 21/22 March 2011, frost was registered at 2 m above ground level (Sosnowiec − 1.3 °C, Wrocław − 1.1 °C). In the upper layers, the temperature was positive.

The temperature gradient in the lower 100-m air layer was very large ($\gamma_{Wrc}100\ m = 7.1$ K; $\gamma_{Sos}100\ m = 5.9$ K). The ID and strength of SBTI reached 198 m and 7.9 K, respectively, in Wrocław. The SBTI also favoured high concentrations of PM_{10} in Gliwice (396 $\mu g \cdot m^{-3}$) on 4 March 2011 and in Dąbrowa Górnicza (357 $\mu g \cdot m^{-3}$) on 5 March 2011. This time, the maximum concentrations of PM_{10} and $PM_{2.5}$ were also registered in Katowice (Table 17).

In summer (JJA), the maximum PM_{10} concentrations (Table 18) rarely exceeded 100 $\mu g \cdot m^{-3}$. The highest concentration of PM_{10} occurred in Dąbrowa Górnicza (171 $\mu g \cdot m^{-3}$) on 26 August 2011 in the anticyclonic SEa situation with the inflow of tropical air (T). All the cases of maximum PM_{10} were favoured by the occurrence of temperature inversion in both the Sosnowiec (γ_{Sos}100 m 1.1–6.4 K 100 m^{-1}) and in Wrocław (γ_{Wrc}100 m 0.8–7.6 K 100 m^{-1}). The thickness of the ID in these situations ranged between 120 and 264 m, and its strength (ΔT_i) ranged between 4.2 and 7.9 K.

In autumn (SON), the maximum PM concentrations were slightly higher (Table 19) than those in spring. In this season, most SBTIs and accompanying high concentrations of PM_{10} were local, as evidenced by the negative values of temperature gradients in Wrocław at the same time. An interesting example is the case of the highest autumn concentration of PM_{10} in Zabrze (535 $\mu g \cdot m^{-3}$) on 10 November 2016, under the isothermal vertical temperature distribution

Table 18 Comparison of the summer maximum PM_{10} concentration (PM_{10} in $\mu g \cdot m^{-3}$) in the Upper Silesia Region with SBTI characteristics in Sosnowiec and Wrocław at 00 UTC (Jan 2001–Sep 2020)

Station	Date	Max PM_{10}	Circulation type	Air mass	γ_{Sos}100 m K·100 m^{-1}	γ_{Wrc}100 m K·100 m^{-1}	ID m	ΔT_i K	γ_i K·100 m^{-1}
Dąbrowa Górnicza PM_{10}	26 Aug 2011	171	SEa	T	1.1	4.1	201	5.2	2.6
Sosnowiec PM_{10}	14 Jul 2016	123	Ka	T/Pmo	5.7	7.6	139	8.0	5.8
Zabrze PM_{10}	14 Aug 2003	120	Wc	Pmo	1.3	1.0	120	1.2	1.0
Gliwice PM_{10}	24 Aug 2002	145	Ea	Pc	6.4	5.0	264	8.2	3.1
Katowice PM_{10}	5 Aug 2004	155	Ec	Pmo	3.5	5.2	211	6.4	3.0
Katowice $PM_{2.5}$	22 Aug 2009	64	Bc	T/Pmo	3.4	0.8	190	1.4	0.7
Average PM_{10} from 5 stations	14 Aug 2003	99	Wc	Pmo	1.3	1.0	120	1.2	1.0

Explanations: as in Tables 7 and 13. Data for Katowice $PM_{2.5}$ are from the shorter period Jun 2009–Sep 2020

Table 19 Comparison of the autumn maximum PM_{10} concentration (Max PM_{10} in μg·m^{-3}) in the Upper Silesia Region with SBTI characteristics in Sosnowiec and Wrocław at 00 UTC (Jan 2001–Sep 2020)

Station	Date	Max PM_{10}	Circulation type	Air mass	γ_{Sos}100 m K·100 m^{-1}	γ_{Wrc}100 m K·100 m^{-1}	ID m	ΔT_i K	γ_i K·100 m^{-1}
Dąbrowa Górnicza PM_{10}	16 Nov 2013	260	NWa	Pmo	2.0	−0.5	-	-	-
Sosnowiec PM_{10}	16 Nov 2013	421	NWa	Pmo	2.0	−0.5	-	-	-
Zabrze PM_{10}	10 Nov 2016	535	Bc	Pmo	−0.2	3.0	154	3.9	2.5
Gliwice PM_{10}	25 Nov 2003	447	SWa	Pmw	7.2	4.3	220	6.0	2.7
Katowice PM_{10}	15 Nov 2011	419	Ka	Pmo	0.9	−0.8	-	-	-
Katowice $PM_{2.5}$	4 Nov 2015	313	Ka	Pc	9.3	10.8	1561	17.1	1.1
Average PM_{10} from 5 stations	15 Nov 2011	311	Ka	Pmo	0.9	−0.8	-	-	-

Explanations: as in Tables 7 and 13. Data for Katowice $PM_{2.5}$ are from the shorter period Jun 2009–Sep 2020

in Sosnowiec. At that time, in Wrocław ID, the SBTI was 154 m thick, and its strength (ΔT_i) reached 3.9 K. This isothermal temperature distribution in the Sosnowiec was due to the fog layer. Therefore, this situation is an example of smog defined as the simultaneous occurrence of high concentrations of PM_{10} (average for Upper Silesia: 228 μg·m^{-3}) near the ground fog.

In autumn, in the period from 25 October to 9 November 2015, there was an extremely long episode of SBTI in southern Poland that formed under the influence of a long-lasting (several days) anticyclonic wedge (Ka) with polar continental air (Pc). In the second part of this period, from 30 October to 7 November 2015, the concentration of PM_{10} in Upper Silesia exceeded 100 μg·m^{-3}. The SBTIs on 3 and 4 November 2015 were exceptional with respect to their strength (ΔT_i = 19.1 K in Wrocław, 00 UTC) and depth (ID = 1254 m). Large SBTIs in the lower 100-m layer of air were found in both Wrocław (γ_{Wrc}100 m = 11.5 K 100 m^{-1}) and in Sosnowiec (γ_{Sos}100 m = 8.2 K 100 m^{-1}). The next day, the SBTI depth (1561 m) was the highest value in the entire research period. The SBTI strength (ΔT_i) was also as large as 17.1 K (Table 19). In this situation, the highest concentration of $PM_{2.5}$ in autumn, amounting to 313 μg·m^{-3}, was recorded in Katowice.

The above-described examples show an apparent influence of SBTIs on PM concentration in the near-ground air layer. This is related to the settling of the air in these situations. To quantify the influence of the air stability in the lowest 100-m layer of the atmosphere and its seasonal variability on air pollution, the averages of PM_{10} concentrations were calculated for three classes of atmospheric stability: instability (γ_{Sos}100 m < −0.5 K), isothermal conditions (γ_{Sos}100 m ≥ −0.5 ^ ≤ 0.5 K), and stable atmosphere with temperature inversions (γ_{Sos}100 m > 0.5 K). In addition to a vertical temperature gradient, weather conditions, mainly wind speed (Grundström et al. 2015b), also significantly impacted the concentration of air pollution.

The annual average PM_{10} concentration (μg·m^{-3}) in the Upper Silesia Region was 49.3 μg·m^{-3}, varying from 27.7 (std ± 13.3) μg·m^{-3} in summer to 72.5 (± 73.2) μg·m^{-3} (± 73.2) in winter (Table 20). In all seasons, the lowest concentrations of PM_{10} were found during unstable

Table 20 Seasonal and annual averages and standard deviations (std) of the PM_{10} concentration (μg·m^{-3}) in the Upper Silesia Region (averages from 5 stations) for the three classes of atmospheric stability in Sosnowiec (γ_{Sos}100 m) at 00 UTC (period Jan 2001–Sep 2020)

γ_{Sos}100 m K 100 m^{-1}	γ_{Sos}100 m < −0.5	γ_{Sos}100 m ≥ −0.5 ^ ≤ 0.5	γ_{Sos}100 m > 0.5	**Average**	γ_{Sos}100 m < −0.5	γ_{Sos}100 m ≥ −0.5 ^ ≤ 0.5	γ_{Sos}100 m > 0.5	No. of data
Season	PM_{10} concentration in μg·m^{-3}				PM_{10} concentration in % of average			
DJF	52.2	53.2	137.2	**72.5**	72.1	73.4	189.2	1701
std	± 46.8	± 47.6	± 101.1	± 73.2				
MAM	31.2	36.6	64.5	**50.1**	62.3	72.9	128.8	1702
std	± 25.1	± 26.5	± 46.5	± 40.5				
JJA	17.2	21.5	31.5	**27.7**	62.3	77.7	113.6	1739
std	± 8.7	± 9.8	± 13.2	± 13.3				
SON	32.6	34.7	64.1	**48.7**	67.0	71.3	131.8	1660
std	± 25.7	± 29.4	± 47.2	± 41.0				
Annual	**40.1**	**37.9**	**61.7**	**49.3**	**81.4**	**76.8**	**125.1**	**6802**
std	± 38.5	± 34.7	± 59.1	± 49.4				

Annual and average data are printed in bold

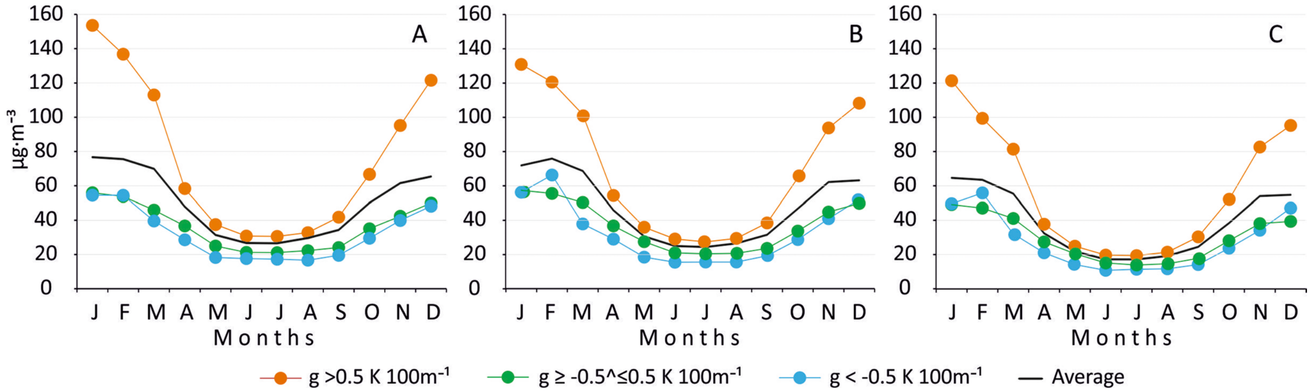

Fig. 9 Annual course of the PM_{10} concentration ($\mu g \cdot m^{-3}$) in the Upper Silesia Region calculated as averages from 5 stations (**A**), Katowice (**B**) and $PM_{2.5}$ in Katowice (**C**) at midnight (00 UTC) for different stability conditions in Sosnowiec ($g = \gamma_{Sos}100$ m). Data for A are for the period Jan 2001–Sep 2020, and for **B** and **C** for Jun 2009–Sep 2020

Table 21 Seasonal and annual averages and standard deviations (std) of the PM_{10} concentration ($\mu g \cdot m^{-3}$) in Katowice for the three classes of atmospheric stability in Sosnowiec ($\gamma_{Sos}100$ m) at 00 UTC (period Jan 2001–Sep 2020)

$\gamma_{Sos}100$ m K 100 m^{-1}	$\gamma_{Sos}100$ m < -0.5	$\gamma_{Sos}100$ m $\geq -0.5 \wedge \leq 0.5$	$\gamma_{Sos}100$ m > 0.5	Average	$\gamma_{Sos}100$ m < -0.5	$\gamma_{Sos}100$ m $\geq -0.5 \wedge \leq 0.5$	$\gamma_{Sos}100$ m > 0.5	No. of data
Season	PM_{10} concentration in $\mu g \cdot m^{-3}$				PM_{10} concentration in % of average			
DJF	53.4	49.5	111.7	**65.4**	81.6	75.7	170.9	1599
std	±45.3	±38.9	±80.5	±58.9				
MAM	31.4	36.5	59.4	**47.5**	66.0	76.9	125.1	1647
std	±25.2	±28.3	±40.3	±36.5				
JJA	15.9	21.8	31.7	**27.8**	57.2	78.4	113.9	1539
std	±8.8	±12.0	±16.1	±16.4				
SON	32.2	33.5	62.0	**46.8**	68.8	71.6	132.5	1542
std	±24.0	±27.6	±51.0	±42.1				
Annual	**40.5**	**36.7**	**57.1**	**47.1**	**86.1**	**78.0**	**121.3**	**6327**
std	±38.3	±33.4	52.0	±44.8				

Annual and average data are printed in bold

atmospheres. In summer, the average concentration of PM_{10} under these conditions was only 17.2 (±8.7) $\mu g \cdot m^{-3}$; in winter, it reached 52.2 (±46.8) $\mu g \cdot m^{-3}$, which constituted 72% of the average winter concentration regardless of the state of the atmosphere. In all seasons, the mean PM_{10} concentrations during temperature inversions were higher than the seasonal means. They ranged from 31.5 (±47.2) $\mu g \cdot m^{-3}$ (114% of the average) in summer to 137.2 (±101.1) $\mu g \cdot m^{-3}$ (189% of the average) in winter.

The annual course of PM_{10} concentration depending on and regardless of air stability is shown in Fig. 9A. During the SBTI, the mean PM_{10} concentrations were lower than 50 $\mu g \cdot m^{-3}$ from May to September, while they were higher than 100 $\mu g \cdot m^{-3}$ from December to March, with a maximum exceeding 150 $\mu g \cdot m^{-3}$ in January. Similar differences were found in Katowice (Table 21) for both PM_{10} (Table 21; Fig. 9B) and $PM_{2.5}$ (Table 22; Fig. 9C) concentrations. In Katowice, the average concentration of $PM_{2.5}$ during the nights with temperature inversion was on average 17% higher than the annual mean, and these values changed from 13% in summer to 71% in winter. For example, in Santiago, Chile (Gramsch et al. 2014), the $PM_{2.5}$ concentration was 35% higher on inversion days than on days without inversion.

Using a large number of measurements (from approximately 950 to over 1800), the relationships between the lapse rate at 100 m ($\gamma_{Sos}100$ m) at 00 UTC in Sosnowiec and the PM_{10} and $PM_{2.5}$ concentrations ($\mu g \cdot m^{-3}$) were investigated in the Upper Silesia region. The calculated coefficients of correlation (r) and determination (r^2*100 in %) are presented in Table 23. In winter, the temperature gradient explained approximately 30% of the variance in the PM_{10} concentration. The coefficient of determination for individual stations ranged from 21% in Katowice to 30% in Sosnowiec. In summer, the averaged coefficient of the determination reached 26% in Zabrze. The

Table 22 Seasonal and annual averages and standard deviations (std) of the $PM_{2.5}$ concentration ($\mu g \cdot m^{-3}$) in Katowice for the three classes of atmospheric stability in Sosnowiec ($\gamma_{Sos}100$ m) at 00 UTC (period Jun 2009–Sep 2020)

$\gamma_{Sos}100$ m K 100 m^{-1}	$\gamma_{Sos}100$ m < -0.5	$\gamma_{Sos}100$ m $\geq -0.5 \wedge \leq 0.5$	$\gamma_{Sos}100$ m > 0.5	Average	$\gamma_{Sos}100$ m < -0.5	$\gamma_{Sos}100$ m $\geq -0.5 \wedge \leq 0.5$	$\gamma_{Sos}100$ m > 0.5	No. of data
Season	$PM_{2.5}$ concentration in $\mu g \cdot m^{-3}$				$PM_{2.5}$ concentration in % of average			
DJF	50.8	45.3	105.2	**61.4**	82.7	73.8	171.4	951
std	±45.3	±38.9	±80.5	±58.9				
MAM	23.8	31.0	44.9	**36.8**	64.7	84.1	122.1	997
std	±18.7	±23.3	±34.0	±30.0				
JJA	11.4	14.7	20.4	**18.0**	63.2	81.6	113.2	1051
std	±6.2	±7.1	±8.9	±8.9				
SON	25.9	28.5	50.9	**38.6**	67.0	73.9	131.8	983
std	±18.1	±22.3	±45.0	±36.4				
Annual	**34.4**	**30.9**	**44.6**	**38.2**	**90.2**	**81.0**	**116.8**	**3982**
std	±35.7	±28.5	±47.5	±40.5				
Annual* PM_{10}	**40.6**	**38.4**	**55.9**	**47.1**	**86.2**	**81.5**	**118.7**	**3977**
std	±38.2	±34.2	±53.1	±45.6				

Explanation: Annual* PM_{10} in Katowice for the same period as $PM_{2.5}$

Annual and average data arer printed in bold

Table 23 Coefficients of correlation (r) and determination (r^2*100 in %) between lapse rate for the 100 m near the ground layer ($\gamma_{Sos}100$ m) at 00 UTC in Sosnowiec, with the PM_{10} and $PM_{2.5}$ concentrations ($\mu g \cdot m^{-3}$) in the Upper Silesia region

Season	Winter DJF		Spring MAM		Summer JJA		Autumn SON		Number of data
Coefficients / Stations	r	r^2*100 %	r	r^2*100 %	r	r^2*100 %	r	r^2*100 %	
Dąbrowa Górnicza	0.51	26	0.33	11	0.27	8	0.33	11	1545–1756
Sosnowiec	0.55	30	0.39	15	0.39	16	0.38	15	1414–1543
Zabrze	0.53	28	0.43	18	0.51	26	0.36	13	1537–1763
Gliwice	0.47	22	0.32	10	0.41	17	0.33	11	1548–1605
Katowice PM_{10}	0.46	21	0.37	14	0.43	18	0.36	13	1635–1782
Katowice $PM_{2.5}$	0.44	19	0.27	7	0.40	16	0.32	10	958–1058
PM_{10} average	**0.55**	**30**	**0.42**	**17**	**0.50**	**25**	**0.39**	**15**	**1754–1840**

$r > 0.32$ are significant at the level $\alpha = 0.001$

Averages for Upper Silesia are printed in bold

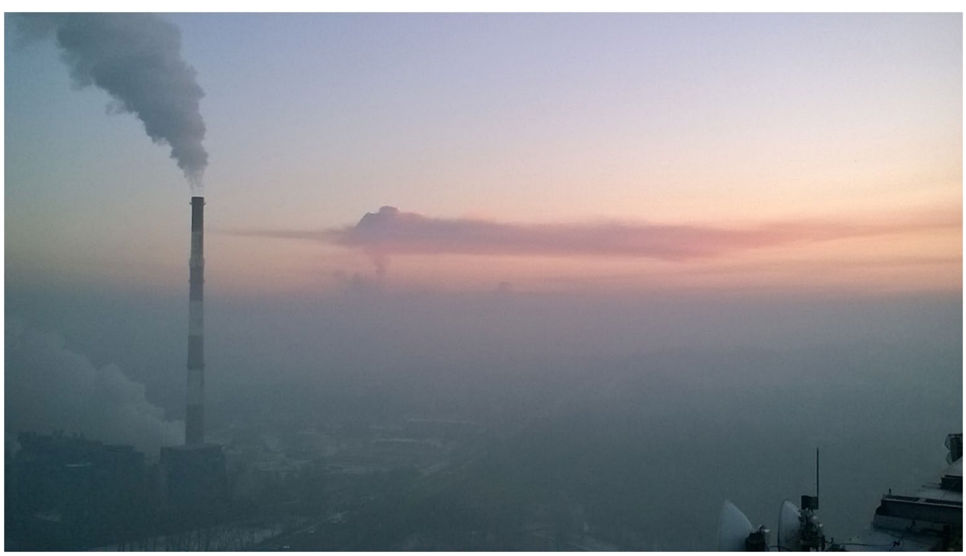

Fig. 10 An example of the smog situation in Sosnowiec on 6 February 2018 at 6:17 UTC. View from the roof of the building of the Institute of Earth Sciences in NE direction (Fot. Tadeusz Niedźwiedź)

relationships were weaker during the transitional seasons (explained variance: 17% in spring and 15% in autumn) and for $PM_{2.5}$ in Katowice (Table 23).

An excellent example of temperature inversion promoted by air subsidence, leading to a high concentration of dust pollutants in the ground layer of the atmosphere during cloudless and frosty weather combined with low wind speed is presented in Fig. 10. The inversion layer also favoured the spreading of pollutants emitted by factory chimneys visible over the Katowice steelworks near Dąbrowa Górnicza. Sometimes, as shown in the photograph, factory chimney smoke can also penetrate the inversion layer.

In Sosnowiec, on 6 February 2018 (Fig. 10), the air temperature at a height of 2 m above the ground at 00 UTC dropped to – 10.6 °C and the lapse rate (γ_{100Sos}) was 4.0 K 100 m^{-1}. According to a radiosonde sounding in Wrocław,

Fig. 11 An example of the smog situation in Sosnowiec on 17 December 2019 at 6:47 UTC. View from the roof of the building of the Institute of Earth Sciences in the S direction (Fot. Tadeusz Niedźwiedź)

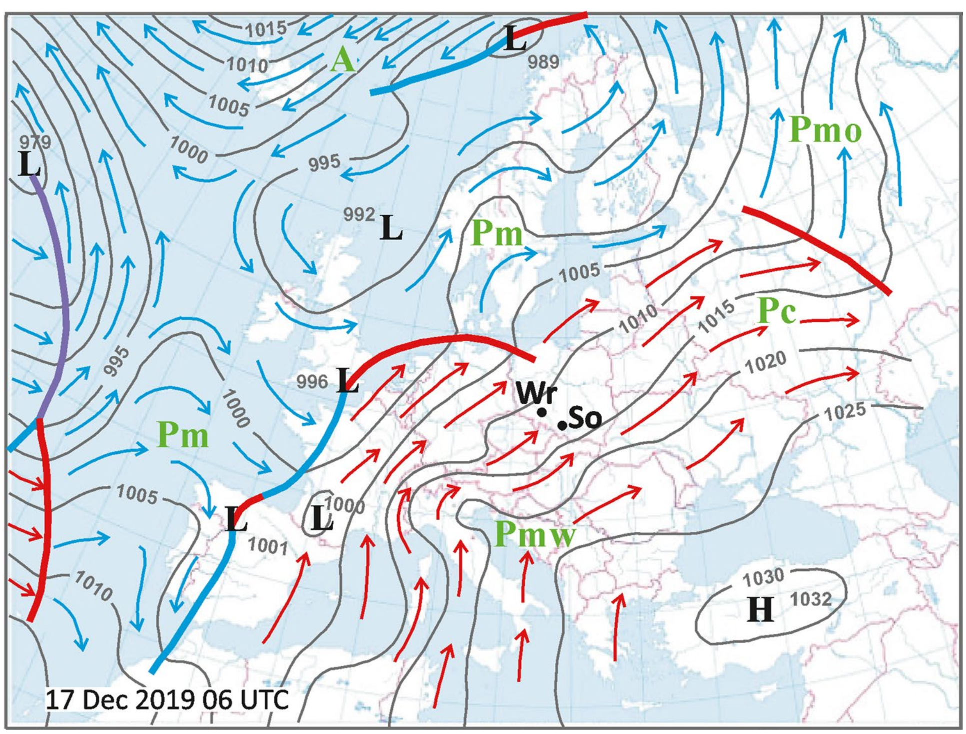

Fig. 12 Synoptic map of Europe 17 Dec 2019 (06 UTC) for the smog situation in Sosnowiec (see Fig. 11). Isobars and atmospheric fronts (blue, cold; red, warm; violet, occlusion) were taken from the synoptic map of the German Meteorological Service (www.wetter3.de/archiv_dwd.html). The arrows indicate the direction of the geostrophic wind in the advection of warm (red) and cool (blue) air. Explanations: L, low centre; H, high centre. Air mass: A, arctic; Pc, polar continental; Pm, polar maritime; Pmo, polar maritime old; Pmw, polar maritime warm; So, Sosnowiec; Wr, Wrocław

the inversion layer was 96 m deep ($\Delta T = 3.8$ K), and the lapse rate was similar to that in Sosnowiec ($\gamma_{100\mathrm{Wrcs}} = 3.8$ K 100 m^{-1}). The discussed air temperature inversion developed during a high-pressure wedge (Ka) in the mass of polar continental air (Pc). The PM_{10} concentration in Sosnowiec at 00 UTC was 233 μg·m^{-3}. In Katowice, between 07 and 09 UTC, the PM_{10} concentration was very high, reaching 153–179 μg·m^{-3}, and for $PM_{2.5}$, it was 132–153 μg·m^{-3}.

Figure 11 shows a photograph illustrating a typical situation with an inverse air temperature distribution and accompanying shallow ground fog in the morning in Sosnowiec. On 17 December 2019, southern Poland was located between a high with a centre located over Turkey and a low with a centre over the Norwegian Sea (Fig. 12). The intensive inflow of a warm air mass (Pmw, polar maritime warm) from the SW (SWc situation, southwest cyclonal) favoured air temperature inversion development during clear sky conditions. In Sosnowiec at 00 UTC, the temperature at 2 m above ground level reached 1.7 °C, while at an altitude of 88 m, the temperature equalled 8.2 °C. Thus, the near-ground lapse rate was considerable ($\gamma_{100\mathrm{Sos}} = 7.5$ K 100 m^{-1}). Similar conditions prevailed in Wrocław, where a temperature inversion with a thickness of 84 m ($\Delta T_{\mathrm{i}} = 7.2$ K; $\gamma_{100\mathrm{Wrc}} = 7.2$ K 100 m^{-1}) developed. On that day, the temperature inversion lasted 24 h.

Such weather conditions favoured an increase in the concentration of air pollution. At 00 UTC PM_{10}, the average concentration from 5 stations was 81 μg·m^{-3}, and in Katowice, it was 91 μg·m^{-3}. The concentration of $PM_{2.5}$, reaching 73 μg·m^{-3}, was relatively high. In the morning at 06–07 UTC, when the photograph in Fig. 11 was taken, the concentration of PM_{10} in Katowice increased significantly up to 147–161 μg·m^{-3}, reaching a maximum of 220 μg·m^{-3} at 09 UTC. On the other hand, the concentration of $PM_{2.5}$ in the hours mentioned above amounted to 120–131 μg·m^{-3} and 173 μg·m^{-3}, respectively. The combination of such a high concentration of particulate matter with fog is an example of a typical smog situation.

4 Conclusions

The strongest surface-based temperature inversions (SBTIs) in southern Poland were observed during nighttime (00 UTC), with an annual frequency of 47–59%. The SBTIs usually developed due to strong radiative cooling of the Earth's surface during a cloudless sky and advection of warm air masses in the higher levels of the atmosphere. The latter condition usually occurred in anticyclonic situations. At midday (12 UTC), the SBTI occurred sporadically (0.6–0.7%), usually only in winter (1.0–2.0%).

In the annual course, the frequency of SBTIs varied from 23–38% in winter to 64–75% in summer, with a higher frequency of clear and windless nights in summer than in winter, when the weather is more dynamic.

According to the sounding data from Wrocław, the annually averaged depth of SBTIs at midnight equalled 207 m, varying from 186 m in spring to 249 m in winter.

Annually, 50% of the SBTI depth fell within the range of 127–146 m, varying from 114–309 m in winter to 131–233 m in summer.

The deepest SBTIs were found in autumn (1561 m) and winter (1388 m). In spring and summer, their maximum thickness did not exceed 750 m.

The influence of SBTIs on the concentrations of particulate matter (PM_{10} and $PM_{2.5}$) was observed mainly in winter and autumn. Exceptionally high concentrations were recorded during frosty nights when the air temperature dropped below – 10 °C or – 15 °C.

The mean annual PM_{10} concentration for the Upper Silesia region at midnight was 49 μg·m^{-3}, ranging from 18 μg·m^{-3} in summer to 73 μg·m^{-3} in winter. During unstable and isothermal conditions, the concentrations of PM_{10} and $PM_{2.5}$ were lower than the average. On the other hand, during nights with a temperature inversion, the annual mean PM_{10} concentrations constituted ca. 125% of the annual mean, ranging from 114% in summer to 189% in winter.

The presented research shows that SBTIs in winter are among the main factors contributing to a high concentration of particulate matter in the near-ground layer of the atmosphere, even during periods with relatively low emissions. The main factor leading to increased PM_{10} concentrations is descending air under inversion conditions during strong cooling of the air layers near the ground due to the negative balance of longwave radiation.

Acknowledgements Radio-sounding data were obtained from the upper air database of the Department of Atmospheric Science, University of Wyoming, USA: weather.uwyo.edu/upperair/ sounding/. html. We also used hourly and daily meteorological data from synoptic stations in Katowice-Muchowiec (WMO no 12560) run by the Institute of Meteorology and Water Management—National Research Institute (IMWM-NRI). The data are stored in the following database: https://dane.imgw.pl/data/dane_pomiarowo_obserwacyjne/dane_meteorologiczne/. Hourly data on standard air pollution concentrations were obtained from the database of the Voivodship Inspectorate for Environmental Protection in Katowice (Wojewódzki Inspektorat Ochrony Środowiska w Katowicach): http://powietrze.katowice.wios.gov.pl/dane-pomiarowe/automatyczne/.

Author contribution Tadeusz Niedźwiedź and Ewa Łupikasza proposed the topic, designed and performed the experimental study, performed the analyses and wrote the paper. Łukasz Małarzewski and Tomasz Budzik helped with the statistical analyses and data interpretation. All authors read and approved the final manuscript.

Funding The research work was funded by the National Science Centre, Poland, under research project no 2017/25/B/ST10/01838 entitled "The influence of temperature inversion in boundary layer atmosphere on air pollution".

Data availability The datasets generated during and/or analysed during the current study are available from the corresponding author on reasonable request.

Code availability Not applicable.

Declarations

Ethics approval Not applicable.

Consent to participate Not applicable.

Consent for publication Not applicable.

Conflict of interest The authors declare no competing interests.

References

Abdul-Wahab SA, Al-Saifi SY, Alrumhi BA, Abdulraheem MY, Al-Uraimi M (2004) Determination of features of the low-level temperature inversions above a suburban site in Oman using radiosonde temperature measurements: Long-term analysis. J Geophys Res 109(D20101):1–9. https://doi.org/10.1029/2004JD004543

Bokwa A (2011) Influence of air temperature inversions on the air pollution dispersion conditions in Krakow. Instytut Geografii i Gospodarki Przestrzennej Uniwersytet Jagielloński. Kraków Prace Geograficzne 126:41–51

Bourne SM, Bhatt US, Zhang J, Thoman R (2010) Surface-based temperature inversions in Alaska from a climate perspective. Atmos Res 95(2–3):353–366. https://doi.org/10.1016/j.atmosres.2009.09.013

Bradley RS, Keimig FT, Diaz HF (1992) Climatology of surface-based inversions in the North American Arctic. J Geophys Res 97(D14):15699–15712. https://doi.org/10.1029/92JD01451

Brümmer B, Lange I, Know H (2012) Atmospheric boundary layer measurements at the 280 m high Hamburg weather mast 1995–2011: mean annual and diurnal cycles. Meteorol Z 21(4):319–335. https://doi.org/10.1127/0941-2948/2012/0338

Brümmer B, Schultze M (2015) Analysis of 7-year low-level temperature inversion data set measured at the 280 m high Hamburg weather MAST. Meteorol Z 324(5):481–494. https://doi.org/10.1127/metz/2015/0669

Caputa ZA, Leśniok MR, Niedźwiedź T, Bil-Knozová G (2009) The influence of atmospheric circulation and cloudiness on the intensity of temperature inversions in Sosnowiec (Upper Silesia. Southern Poland). Int J Environ Waste Manag 4(1/2):17–31. https://doi.org/10.1504/IJEWM.2009.026881

Czarnecka M, Nidzgorska-Lencewicz J (2017) The impact of thermal inversion on the variability of PM concentration in winter seasons in Tricity. Environ Prot Eng 43(2):157–172. https://doi.org/10.37190/epe170213

Czarnecka M, Nidzgorska-Lencewicz J, Rawicki K (2019) Temporal structure of thermal inversions in Łeba (Poland). Theoret Appl Climatol 136(1–2):1–13. https://doi.org/10.1007/s00704-018-2459-8

Feng X, Wei S, Wang S (2020) Temperature inversions in the atmospheric boundary layer and lower troposphere over the Sichuan Basin, China: Climatology and impact on air pollution. Sci Total Environ 726:138579. https://doi.org/10.1016/j.scitotenv.2020.138579

Fochesatto GJ (2015) Methodology for determining multilayered temperature inversions. Atmos Meas Tech 8:2051–2026. https://doi.org/10.5194/amt-8-2051-2015

Glickman TS (ed) (2000) Glossary of meteorology, 2nd edn. American Meteorological Society, Boston, p 855

Gramsch E, Cáceres D, Oyola P, Reyes F, Vásquez Y, Rubio MA, Sánchez G (2014) Influence of surface and subsidence thermal inversion on $PM_{2.5}$ and black carbon concentration. Atmos Environ 98:290–298. https://doi.org/10.1016/j.atmosenv.2014.08.066

Grundström M, Tang L, Hallquist M, Nguyen H, Chen D, Pleijel H (2015a) Influence of atmospheric circulation patterns on urban air quality during the winter. Atmos Pollut Res 6(2):278–285. https://doi.org/10.5094/APR.2015.032

Grundström M, Hak C, Chen D, Hallquist M, Pleijel H (2015b) Variation and co-variation of PM_{10} particle number concentration NO_x and NO_2 in the urban air - relationships with wind speed, vertical temperature gradient and weather type. Atmos Environ 120:317–327. https://doi.org/10.1016/j.atmosenv.2015.08.057

Gutsche A (1983) Die Andauer von Inversionen an den aerologischen Stationen der Bundersepublik Deutschland. Deutsche Meteorologen-Tagung. Von 16. Bis. 19. Mai 1983 in Bad Kissingen. Annalen der Meteorologie (Neue Folge) 20:79-81

Janhäll S, Olofson KFG, Anderson PU, Pettersson JBC, Hallquist M (2006) Evolution of the urban aerosol during winter temperature inversion episodes. Atmos Environ 40(28):5355–5366. https://doi.org/10.1016/j.atmosenv.2006.04.051

Kahl JD (1990) Characteristics of the low-level temperature inversion along the Alaskan Arctic coast. Int J Climatol 10(5):537–548. https://doi.org/10.1002/joc.3370100509

Kamińska JA (2017) Zjawisko smogu na tle jakości powietrza we Wrocławiu w latach 2012–2016 (The smog phenomenon and the air quality in Wrocław in 2012–2016). Inżynieria Ekologiczna (Ecological Engineering) 18(5):66–76 (in Polish. Abstract in English)

Kassomenos PA, Koletsis IG (2005) Seasonal variation of the temperature inversions over Athens, Greece. Int J Climatol 25(12):1651–1663. https://doi.org/10.1002/joc.1188

Kassomenos PA, Paschalidou AK, Lykoudis S, Koletsis I (2014a) Temperature inversion characteristics in relation to synoptic circulation above Athens, Greece. Environ Monit Ass 186(6):3495–3502. https://doi.org/10.1007/s10661-014-3632-x

Kassomenos PA, Vardoulakis S, Chaloulakou A, Paschalidou AK, Grivas G, Borge R, Lumbreras J (2014b) Study of PM_{10} and $PM_{2.5}$ levels in three European cities: analysis of intra and inter urban variations. Atmos Environ 87:153–163. https://doi.org/10.1016/j.atmosenv.2014.01.004

Katsoulis BD (1988) Aspects of the occurrence of persistent surface inversions over Athens Basin, Greece. Theoret Appl Climatol 39:98–107. https://doi.org/10.1007/BF00866395

Lamb HH (1972) British Isles weather types and a register of the daily sequence of circulation patterns, 1861–1971. Geophys Mem 116:1–85

Largeron Y, Staquet C (2016) Persistent inversion dynamics and wintertime PM_{10} air pollution in Alpine valleys. Atmos Environ 135:92–108. https://doi.org/10.1016/j.atmosenv.2016.03.045

Leśniok MR, Caputa ZA (2009) The role of atmospheric circulation in air pollution distribution in Katowice Region (Southern Poland). Int J Environ Waste Manage 4(1/2):17–31. https://doi.org/10.1504/IJEWM.2009.026881

Leśniok M, Małarzewski Ł, Niedźwiedź T (2010) Classification of circulation types for Southern Poland with an application to air pollution concentration in Upper Silesia. Phys Chem Earth 35(9–12):516–522. https://doi.org/10.1016/j.pce.2009.11.006

Li J, Chen HB, Li ZQ, Wang CP, Cribb M, Fan XH (2015) Low-level temperature inversion and their effect on aerosol condensation nuclei concentrations under different large-scale synoptic circulations. Adv Atmos Sci 32(7):898–908. https://doi.org/10.1007/s00376-014-4150-z

Li J, Chen H, Li Z, Wang P, Fan X, He W, Zhang J (2019) Analysis of low-level temperature inversions and their effects on aerosols in the lower atmosphere. Adv Atmos Sci 36(11):1235–1250. https://doi.org/10.1007/s00376-019-9018-9

Liu Y, Zhao N, Vanos JK, Cao G (2017) Effect of synoptic weather on ground-level $PM_{2.5}$ concentrations in the United States. Atmos Environ 148:297–305. https://doi.org/10.1016/j.atmosenv.2016.10.052

Lokoshchenko MA (2002) Long-term sodar observations in Moscow and a new approach to potential mixing determination by radiosonde data. J Atmos Oceanic Tech 19(8):1151–1162. https://doi.org/10.1175/1520-0426(2002)019%3c1151:LTSOIM%3e2.0.CO;2

Malingowski J, Attkinson D, Fochesatto J, Cherry J, Stevens E (2014) An observational study of radiation temperature inversions in Fairbanks, Alaska. Polar Sci 8(1):24–39. https://doi.org/10.1016/j.polar.2014.01.002

Milionis AE, Davies TD (2008) The effect of the prevailing weather on the statistics of atmospheric temperature inversions. International Journal of Climatology 28(10):1385–1397. Published online 11 October 2007 in Wiley InterScience (www.interscience.wiley.com).https://doi.org/10.1002/joc.1613

Niedźwiedź T, Łupikasza E (2019) Atmospheric circulation in the investigations of Polish climatologists. Przegląd Geofizyczny 64(1–2):1–58. https://doi.org/10.32045/PG-2019-004 ((**Englishversion**))

Olofson KFG, Andersson PU, Hallquist M, Ljungström E, Tang L, Chen D, Pettersson JBC (2009) Urban aerosol evolution and particle formation during wintertime temperature inversions. Atmos Environ 43(2):340–346. https://doi.org/10.1016/j.atmosenv.2008.09.080

Palarz A, Ustrnul Z, Wypych A (2015) Temperature inversions in the Polish Carpathians and their influence on air pollution (case study). In Šiška et al. (eds): Towards Climatic Services. Nitra. Slovakia. 15th - 18th September 2015: 1–6

Palarz A, Celiński-Mysław D (2017) The effect of temperature inversions on the particulate matter PM_{10} and sulfur dioxide concentrations in selected basins in the Polish Carpathians. Carpath J Earth Environ Sci 12(2):629–640. Accessed December 2020 https://www.researchgate.net/publication/317283683

Palarz A, Celiński-Mysław D, Ustrnul Z (2018) Temporal and spatial variability of surface based inversions over Europe based on ERA-Interim reanalysis. Int J Climatol 38(1):158–168. https://doi.org/10.1002/joc.5167

Pleijel H, Grundström M, Karlsson GP, Karlsson PE, Chen D (2016) A method to assess the inter-annual weather-dependent variability in air pollution concentration and deposition based on weather typing. Atmos Environ 126:200–210. https://doi.org/10.1016/j.atmosenv.2015.11.053

Prezerakos NG (1998) Lower tropospheric structure and synoptic scale circulation patterns during prolonged temperature inversions over Athens, Greece. Theoret Appl Climatol 60(1–4):63–76

Seidel DJ, Ao CO, Li K (2010) Estimating climatological planetary boundary layer heights from radiosonde observations: comparison of methods and uncertainty analysis. J Geophys Res 115(D16113):1–15. https://doi.org/10.1029/2009JD013680

Serreze MC, Schnell RC, Kahl JD (1992) Low-level temperature inversions of the Eurasian Arctic and comparisons with Soviet drifting station. J Clim 5(6):615–629. https://doi.org/10.1175/1520-0442(1992)005%3c0615:LLTI-OT%3e2.0.C);2

Sheridan SC, Powerb HC, Senkbeil JC (2008) A further analysis of the spatio-temporal variability in aerosols across North America: Incorporation of lower tropospheric (850-hPa) flow. Int J Climatol 28(9):1189–1199. https://doi.org/10.1002/joc.1628

Stryhal J, Huth R, Sládek I (2017) Climatology of low-level temperature inversions at the Prague-Libuš aerological station. Theoret Appl Climatol 127(1–2):409–420. https://doi.org/10.1007/s00704-015-1639-z

Tavousi T, Abadi NH (2016) Investigation of inversion characteristics in atmospheric boundary layer: a case study of Teheran, Iran. Modelling Earth System and Environment 2(85). Accessed 18 May 2021 https://doi.org/10.1007/s40808-016-0139-1

Twardosz R, Niedźwiedź T (2001) Influence of synoptic situations on the precipitation in Kraków (Poland). Int J Climatol 21(4):467–481. https://doi.org/10.1002/joc.620

Twardosz R, Niedźwiedź T, Łupikasza E (2011) The influence of atmospheric circulation on the type of precipitation (Kraków, southern Poland). Theoret Appl Climatol 104(1–2):233–250. https://doi.org/10.1007/s00704-010-0340-5

Wang XY, Wang KC (2014) Estimation of atmospheric mixing layer height from radiosonde data. Atmos Meas Tech 7(6):1701–1709. https://doi.org/10.5194/amt-7-1701-2014

Widawski A (2015) The influence of atmospheric circulation on the air pollution concentration and temperature inversion in Sosnowiec. Case Study. Environ Socio-Econom Stud 3(2):30–40. https://doi.org/10.1515/environ-2015-0060

Wolf T, Esau I, Reuder J (2014) Analysis of the vertical temperature structure in the Bergen valley Norway and its connection to pollution episodes. J Geophys Res-Atmos 119(18):10645–10662. https://doi.org/10.1002/1014JD022085

Woś A (2010) Klimat Polski w drugiej połowie XX wieku (Climate of Poland in the second half of the 20th century). Wydawnictwo Naukowe UAM, Poznań 489 pp. (in Polish, summary in English)

Zhang Y, Seidel DJ, Golaz JC, Deser C, Tomas RA (2011) Climatological characteristics of Arctic and Antarctic surface-based inversions. J Clim 24(19):5167–5186. https://doi.org/10.1175/2011JCLI4004.1